Hepatic AKAP1 deficiency exacerbates diet-induced MASLD by enhancing GPAT1-mediated lysophosphatidic acid synthesis

Linjie He[1,7], Xiaojuan She[1,2,7], Lifei Guo[1,3], Mingshu Gao[3,4], Shuangbin Wang[4,5], Zhenxing Lu[1], Haitao Guo[1], Renlong Li[6], Yongzhan Nie[6], Jinliang Xing[1] ✉ & Lele Ji[4] ✉

Metabolic dysfunction-associated steatotic liver disease (MASLD), closely associated with obesity, can progress to metabolic dysfunction-associated steatohepatitis when the liver undergoes overt inflammatory damage. A-kinase anchoring protein 1 (AKAP1) has been shown to control lipid accumulation in brown adipocytes. However, the role of AKAP1 signaling in hepatic lipid metabolism and MASLD remains poorly understood. Here, we showed that hepatocyte-specific AKAP1 deficiency exacerbated hepatic steatosis and steatohepatitis in male mice subjected to a high-fat diet and fast-food diet, respectively. Mechanistically, AKAP1 directly phosphorylated and inactivated glycerol-3-phosphate acyltransferase 1 (GPAT1) in a PKA-dependent manner, thus suppressing lysophosphatidic acid (LPA) production. Increased endogenous LPA in hepatocytes promoted hepatocellular triglyceride (TG) synthesis and initiated pronounced inflammatory response in Kupffer cells. Restoring hepatic AKAP1 or repressing LPA levels via *GPAT1* knockdown alleviated MASLD exacerbation. Overall, AKAP1 plays a protective role against MASLD by inhibiting GPAT1 activity, highlighting the potential of targeting AKAP1/PKA/GPAT1 signalosome for MASLD therapy.

Metabolic dysfunction-associated steatotic liver disease (MASLD), also known as nonalcoholic fatty liver disease (NAFLD), is a prevalent etiology of chronic hepatic disorders, encompassing a wide range of manifestations from simple steatosis to metabolic dysfunction-associated steatohepatitis (MASH) and cirrhosis. The prevalence of MASLD is a significant public health concern in both developed and developing countries, impacting approximately 25% of the global population[1]. As of now, only resmetirom has been approved by the FDA to treat MASH with moderate to advanced liver fibrosis. However, the long-term efficacy and safety still require further evaluation through clinical trials[2,3]. The mechanisms underlying MASLD onset and progression are still imperative to elucidate.

A primary driver of MASLD and MASH is the hepatic overload of key metabolic substrates, carbohydrates and fatty acids (FA), leading to accumulation of toxic lipid species. These lipotoxic lipids induce hepatocellular stress, apoptosis and death, resulting in the development of MASH characterized by hepatocellular injury, inflammation, stellate cell activation, and progressive accumulation of excess extracellular matrix[4]. Hepatic steatosis occurs when fatty acid oxidation (FAO) and lipid export fail to offset the increased fatty acid uptake and

[1]State Key Laboratory of Holistic Integrative Management of Gastrointestinal Cancers and Department of Physiology and Pathophysiology, Fourth Military Medical University, Xi'an, Shaanxi, China. [2]College of Life Sciences, Yan'an University, Yan'an, Shaanxi, China. [3]College of Life Sciences, Northwest University, Xi'an, Shaanxi, China. [4]National Demonstration Center for Experimental Basic Medical Science Education, Fourth Military Medical University, Xi'an, Shaanxi, China. [5]Medical College of Yan'an University, Yan'an, Shaanxi, China. [6]State Key Laboratory of Holistic Integrative Management of Gastrointestinal Cancers and National Clinical Research Center for Digestive Diseases, Xijing Hospital of Digestive Diseases, Fourth Military Medical University, Xi'an, Shaanxi, China. [7]These authors contributed equally: Linjie He, Xiaojuan She. ✉e-mail: xingjl@fmmu.edu.cn; jilele@fmmu.edu.cn

synthesis. Therefore, clarifying the fates of FA in hepatocytes is crucial for understanding the metabolic basis of MASH. In hepatocytes, the increased FA need to be activated by the acyl-CoA synthetases (ACS) to form acyl-CoAs and then undergo either β-oxidation or re-esterification into glycerolipids and phospholipids. Glycerol-3-phosphate acyltransferase 1 (GPAT1), a mitochondrial outer membrane (OMM) protein encoded by *GPAM*, converts the newly formed acyl-CoAs into lysophosphatidic acid (LPA) and prevents their conversion to acyl-carnitines. Thus, it has been proposed that the GPAT1 might serve as a valve that diverts acyl-CoAs away from β-oxidation and toward triglyceride (TG) synthesis[5,6]. Recent GWASs have also demonstrated that loss of function variants in *GPAM* manifest a protective effect on the risk of MASLD in humans[7–9]. These studies have illustrated the existence of a close relationship between GPAT1 and MASLD development, and a better knowledge of the regulation factors that control the activity of this enzyme may help the development of potential therapeutic approaches for MASLD.

A-kinase anchoring protein 1 (AKAP1) serves as a scaffold protein that recruits protein kinase A (PKA), along with other signaling proteins and RNA, to the OMM[10]. It integrates intercellular signal transduction cascades to maintain mitochondrial networks and bioenergetics, cellular calcium homeostasis, and viability[11]. Therefore, AKAP1 could promote the assembly of signalosomes on the OMM and act as a central hub for mitochondrial signaling. Several studies using AKAP1 knockout mice have elucidated the role of AKAP1 in supporting cardiovascular, lung and neuronal cell survival in the stressful environment[12,13]. We have previously reported that AKAP1 represses β-oxidation in brown adipocytes and promotes diet-induced obesity[14]. However, the role of AKAP1 in the development MASLD and the mechanisms by which AKAP1 regulates hepatic lipid metabolism remain uncertain.

Here, we reported the surprising findings that AKAP1 had no impact on FAO but significantly inhibited TG synthesis in hepatocytes via phosphorylating and inactivating the key rate-limiting enzyme GPAT1 in a PKA-dependent manner. Hepatocyte-specific AKAP1 deficiency exacerbated hepatic steatohepatitis in a fast-food diet (FFD)-induced mouse MASH model, while restoration of AKAP1 in the liver rescued the exacerbated MASH in hepatocyte-specific AKAP1 deficient mice. Mechanistically, the LPA derived from GPAT1 served as a crucial mediator in hepatic TG synthesis and liver inflammation in the context of AKAP1 deficiency. These findings indicate that the AKAP1 signalosome establishes a microdomain with elevated PKA activity on the OMM, precisely governing the destiny of acyl-CoAs, thereby regulating TG synthesis and liver inflammation.

Results

Hepatocyte-specific AKAP1 deficiency exacerbates HFD-induced steatosis and FFD-induced MASH in mice

To investigate the specific role of hepatic AKAP1 in the pathogenesis of MASLD, we employed a CRISPR-Cas9 approach combined with a Cre-loxP recombination system to generate mice with conditional knockout of AKAP1 (AKAP1-Flox). Hepatocyte-specific AKAP1 knockout mice (AKAP1-HKO) were generated by crossing albumin-cre transgenic and AKAP1-Flox mice (Supplementary Fig. 1a). Western blotting demonstrated that AKAP1 was successfully knocked out in liver tissue of AKAP1-HKO mice compared to those of AKAP1-Flox mice, but not in other tissues (Supplementary Fig. 1b). Upon NCD feeding, no significant differences were observed between AKAP1-HKO and AKAP1-Flox mice. As lipotoxicity is the leading cause of MASLD initiation[15], we investigated the function of AKAP1 in a mouse MASLD model based on 24 weeks of HFD feeding. Prolonged HFD resulted in increases in body weight, blood glucose levels, insulin resistance, serum TG and TC levels, metabolic tissues weight (adipose tissue mass, heart weight and liver weight) (Supplementary Figs. 2a–d and 3a, b). However, AKAP1-HKO mice showed elevated serum TG levels and increased liver

weights (Supplementary Fig. 2c–e) compared to AKAP1-Flox mice upon HFD feeding. H&E staining (Supplementary Fig. 2f), Oil Red O staining (Supplementary Fig. 2g) and measurements of liver TG and TC contents (Supplementary Fig. 2h) revealed that AKAP1-HKO mice exhibited accelerated hepatic steatosis in response to HFD feeding. Furthermore, HFD-induced serum ALT and AST levels were further increased in AKAP1-HKO mice (Supplementary Fig. 2i). These findings reveal that *AKAP1* genetic deletion aggravates HFD-induced hepatic steatosis and hepatocellular injury.

Given that MASH is the advanced stage of MASLD[4], we also examined the effect of hepatocyte AKAP1 disruption on the MASH progression caused by a prolonged fast-food diet (FFD, a western diet plus a total of 42 g/L of carbohydrate mixed in drinking water at a ratio of 45% glucose and 55% fructose)[16]. After 16 weeks of FFD feeding, both AKAP1-Flox mice and AKAP1-HKO mice exhibited similar increases in body weight, blood glucose levels, insulin resistance, serum TG and TC levels, heart weight, kidney weight and adipose tissue mass (Fig. 1a–d and Supplementary Fig. 3c, d). Furthermore, AKAP1-Flox mice developed MASH in a similar pattern to that observed in humans, showing increased liver weight (Fig. 1d, e), NAFLD activity scores (NAS, histological scoring of steatosis, lobular inflammation, and ballooning) (Fig. 1f), Oil Red O positive area (Fig. 1g), fibrosis severity scores (Fig. 1h) and hepatic inflammation (Fig. 1i) with concomitant obesity as well as dyslipidemia and insulin resistance. More severe hepatic steatosis (Fig. 1f) and increased hepatic lipid content (Fig. 1j, k) were observed in the livers of FFD-fed AKAP1-HKO mice compared to those in FFD-fed AKAP1-Flox mice. Moreover, the hepatic lipid accumulation was more pronounced in FFD-fed AKAP1-HKO mice than that in the HFD-fed AKAP1-HKO mice (Fig. 1j, k and Supplementary Fig. 2h). Furthermore, after FFD feeding, AKAP1-HKO mice developed markedly aggravated fibrosis, as indicated by increased fibrosis severity scores (Fig. 1h) and α-SMA (a marker of HSC activation)-positive regions (Supplementary Fig. 3f). Consistently, AKAP1-HKO mice presented remarkably accelerated hepatic inflammation, as indicated by the evident infiltration of F4/80-positive inflammatory cells compared with the AKAP1-Flox mice after FFD feeding (Fig. 1i). RT-qPCR results further revealed that the expression of genes associated with fibrosis (*Col1a1, Col3a1, Tgfb* and *α-Sma*) and inflammation (*Il1b, Il6, Tnfα* and *Mcp1*) was significantly elevated in the liver of AKAP1-HKO mice compared with AKAP1-Flox mice after FFD feeding (Supplementary Fig. 3e, g). In addition, AKAP1-HKO mice exhibited higher serum ALT and AST levels compared to the AKAP1-Flox mice after FFD feeding (Fig. 1l, m). Collectively, these findings indicate that hepatocyte-specific AKAP1 deficiency has minimal effect on whole-body metabolism but lead to more severe MASH phenotypes following FFD feeding.

Restoration of hepatic AKAP1 expression rescues the exacerbated MASH in AKAP1-HKO mice

To further confirm the correlation of hepatic AKAP1 expression with MASH progression, we generated an AKAP1 expression vector using adeno-associated virus (AAV) type 8 (AAV8-AKAP1). AKAP1-Flox mice and AKAP1-HKO mice (8 weeks of age) were fed on FFD for 4 weeks, followed by intravenous tail injection of AAV8-AKAP1 to specifically overexpress and restore liver AKAP1 levels, respectively. After an additional 12 weeks of FFD feeding, mice were euthanized and analyzed (Fig. 2a). Western blotting demonstrated that tail vein injection of AAV8-AKAP1 successfully upregulated AKAP1 expression in the livers, but not in other tissues (Fig. 2b, Supplementary Fig. 4). There were no significant differences in body weight, serum TG and TC levels among the four groups (Fig. 2c, d). In AKAP1-HKO mice, AKAP1 restoration significantly alleviated FFD-induced hepatic steatosis, as evidenced by decreased liver weight (Fig. 2e), NAFLD activity scores (NAS) (Fig. 2f), Oil Red O positive staining (Fig. 2g) and liver TG and TC contents (Fig. 2j, k). Furthermore, fibrosis severity scores as evaluated by Masson's trichrome staining (Fig. 2h), inflammatory responses as
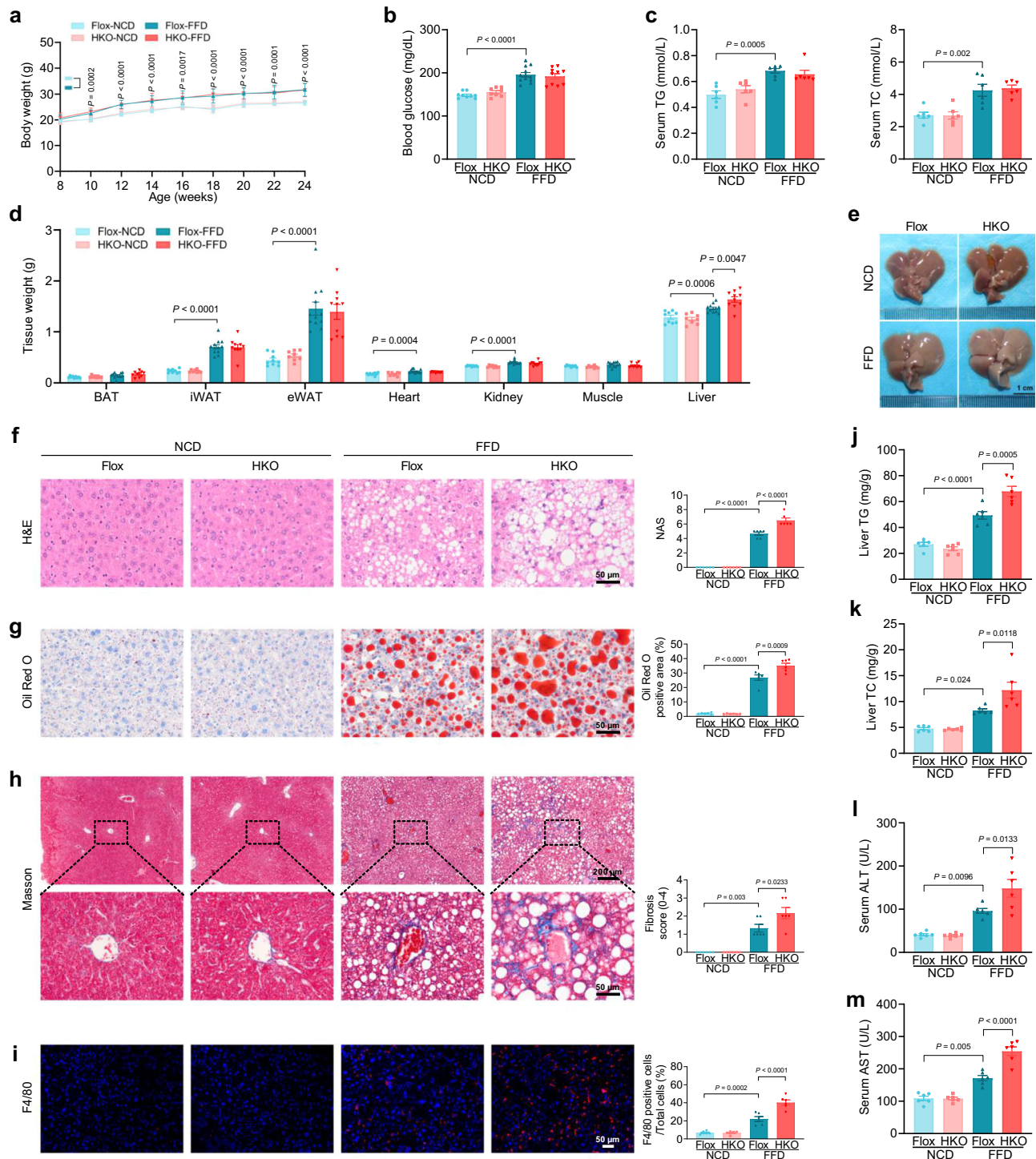
Fig. 1 | Hepatocyte-specific AKAP1 deficiency exacerbates FFD-induced MASH in mice. AKAP1-Flox and AKAP1-HKO male mice were fed on NCD or FFD for 16 weeks. **a** Sequential changes in body weight. **b** Blood glucose levels. **c** Serum TG and TC levels. **d** Tissue weight. **e** Representative images of liver dissected from mice in the indicated groups. Scale bar, 1 cm. **f** Representative H&E-staining images (left) and NAFLD activity score (NAS) of each group (right). Scale bar, 50 μm. **g** Representative Oil Red O staining images (left) and quantification of the Oil Red O positive area (right). Scale bar, 50 μm. **h** Representative Masson's Trichrome staining images (left) and fibrosis score (right). Upper scale bar, 200 μm; lower scale bar, 50 μm. **i** Representative immunofluorescence staining images of F4/80 (left) and quantification of the F4/80 positive cells (right). Scale bar, 50 μm. **j, k** Liver TG and TC levels. **l, m** Serum ALT and AST levels. For (**a**), (**b**) and (**d**), $n = 9$ AKAP1-Flox mice and $n = 8$ AKAP1-HKO mice for the NCD group; $n = 12$ AKAP1-Flox mice and $n = 10$ AKAP1-HKO mice for the FFD group. For (**c**) and (**f**–**n**), $n = 6$ mice per group. Data were expressed as mean ± SEM. Two-way repeated-measures ANOVA followed by Bonferroni post hoc analysis for (**a**); one-way ANOVA with Bonferroni post hoc analysis for (**b**–**d**, **f**–**m**). NCD, normal control diet, Source data are provided as Source Data file.
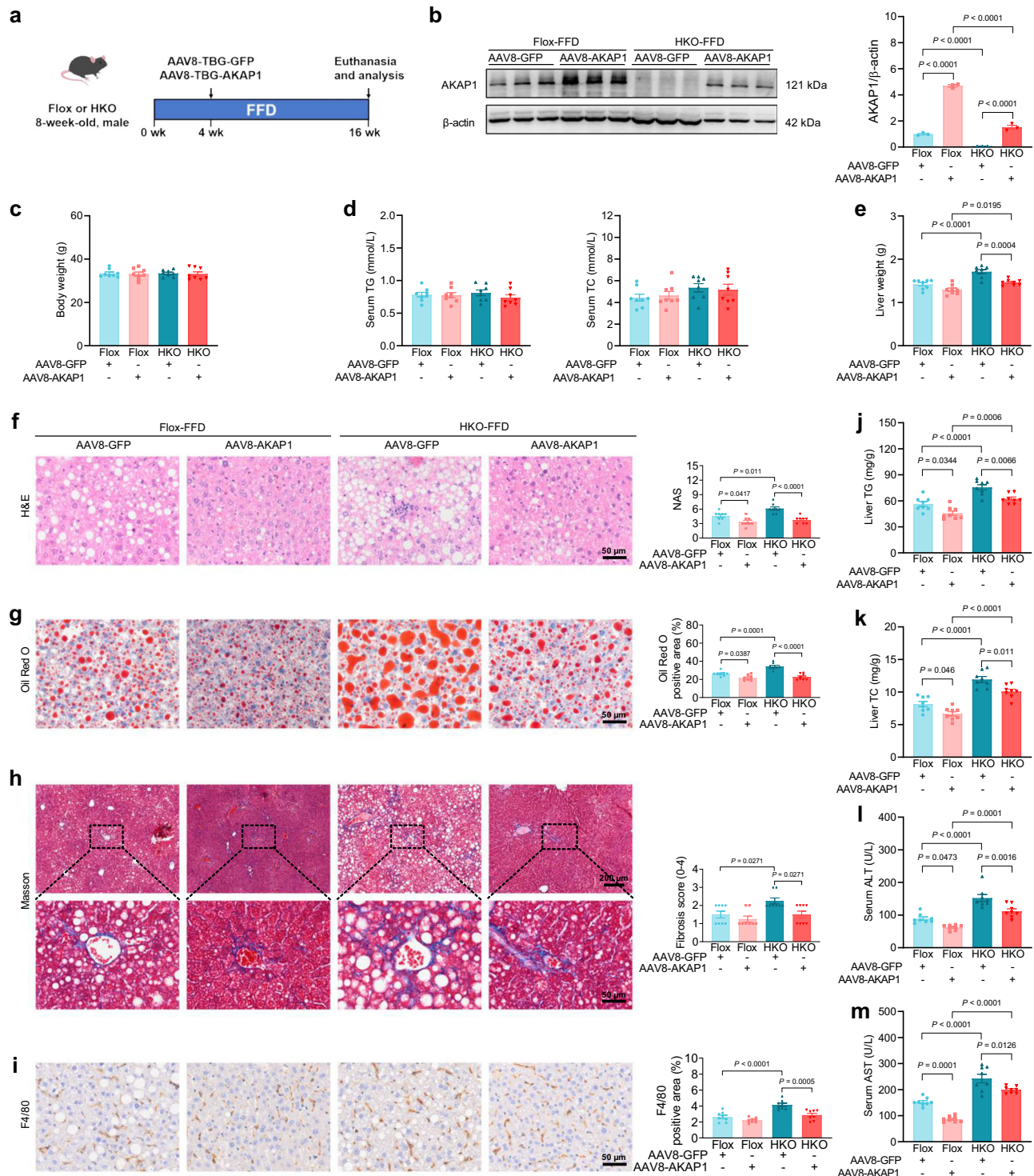
Fig. 2 | Restoration of hepatic AKAP1 expression rescues the exacerbated MASH in AKAP1-HKO mice. a AKAP1-Flox mice and AKAP1-HKO mice (8 weeks of age) were fed on FFD for 4 weeks, followed by intravenous tail injection of AAV8-TBG-AKAP1 to specifically overexpress and restore liver AKAP1 levels, respectively. After an additional 12 weeks of FFD feeding, mice were euthanized and analyzed. **b** Western blotting analysis of AKAP1 protein expression. β-actin was used as a loading control. **c** Body weight. **d** Serum TG and TC levels. **e** Liver weight. **f** Representative H&E-staining images (left) and NAFLD activity score (NAS) of each group (right). Scale bar, 50 μm. **g** Representative Oil Red O staining images (left)

and quantification of the Oil Red O positive area (right). Scale bar, 50 μm. **h** Representative Masson's Trichrome staining images (left) and fibrosis score (right). Upper scale bar, 200 μm; lower scale bar, 50 μm. **i** Representative immunohistochemical staining images of F4/80 (left) and quantification of the F4/80 positive area (right). Scale bar, 50 μm. **j, k** Liver TG and TC levels. **l, m** Serum ALT and AST levels. For (**b**), $n = 3$ mice per group. For (**c–m**), $n = 8$ mice per group. Data were expressed as mean ± SEM. One-way ANOVA with Bonferroni post hoc analysis for all data. Source data are provided as Source Data file.

indicated by F4/80 IHC (Fig. 2i), and the levels of serum biomarkers of liver injury (ALT and AST, Fig. 2l, m) were also substantially decreased by AKAP1 restoration in AKAP1-HKO mice, indicating that AKAP1 restoration markedly decreased FFD-induced steatohepatitis. These results further indicate that restoration of AKAP1 improves MASH in AKAP1-HKO mice, suggesting a critical role of AKAP1 in the progression of MASH. In addition, elevated AKAP1 expression in the Flox+AAV8-AKAP1 group significantly reduced hepatic TG and TC levels, and decreased serum ALT and AST levels compared to both the Flox+AAV8-GFP and HKO + AAV8-AKAP1 groups (Fig. 2j–m). These results indicate that AKAP1 overexpression beyond physiological levels confers protective effects, particularly by reducing lipid accumulation and alleviating hepatocellular damage. However, increased AKAP1 expression in the Flox+AAV8-AKAP1 group had no significant impact on liver fibrosis or inflammation, potentially due to the inherently low baseline levels observed in the Flox+AAV8-GFP group.

Hepatocyte-specific AKAP1 deficiency promotes hepatic steatosis by upregulating TG synthesis

Hepatic lipid accumulation can arise from increased lipid synthesis, elevated fatty acid uptake, impaired β-oxidation, reduced secretion via VLDL, or a combination of these abnormalities. To investigate the mechanism underlying the impact of AKAP1 on hepatic steatosis, we examined the expression of genes involved in these processes. As depicted in Fig. 3a, the mRNA levels of genes encoding proteins involved in de novo lipogenesis (DNL) and in TG synthesis were significantly elevated in HKO mice compared to flox littermates after FFD feeding. No differences were observed in the mRNA levels involved in fatty acid uptake, FAO or VLDL secretion between HKO and flox littermates. Western blotting analysis confirmed that ACC1, FASN, MGAT1 and DGAT2 protein levels in liver tissue were significantly increased in AKAP1-HKO mice compared to their controls (Fig. 3b, c). Furthermore, a lipidomic analysis of the livers were performed in AKAP1-HKO mice and flox littermates following FFD feeding. Several lipid classes changed, most pronounced of which was an increase in total TG abundance in liver from AKAP1-HKO mice as compared with flox littermates (Fig. 3d–f). Similarly, higher levels of diglyceride (DG) were detected in liver from AKAP1-HKO as compared with flox mice (Fig. 3d–f). In contrast, the levels of phosphatidylethanolamine (PE), cardiolipin (CL) and sphingomyelin (SM) were significantly decreased in liver from AKAP1-HKO mice (Fig. 3d–f). Collectively, these data indicate that hepatocyte-specific AKAP1 deficiency accelerates FFD-induced TG synthesis, and also regulates content of phospholipids in liver.

In parallel, we evaluated the role of hepatic AKAP1 in the regulation of hepatic fatty acid uptake. Fatty acid uptake is a multifaceted process that necessitates the coordinated actions of transmembrane transporters, lipid-binding proteins and enzymes, which collectively facilitate the cellular import and intracellular distribution of exogenous FA. Our data showed that mRNA and protein expression levels of fatty acid translocase (CD36/FAT), fatty acid transport proteins (FATP1, FATP2, FATP5), fatty acid binding protein 1 (FABP1), and acyl-CoA synthases (ACSL1, ACSL3) were comparable between the two groups (Fig. 3a and Supplementary Fig. 5a). Moreover, AKAP1 deficiency did not lead to CD36 translocation to the plasma membrane in hepatocytes (Supplementary Fig. 5a). These data indicated that hepatocyte-specific AKAP1 deficiency did not affect fatty acid uptake after FFD. Next, we assayed hepatic FAO by determining FAO-related protein expressions and palmitoyl carnitine levels in livers from FFD-fed AKAP1-HKO and flox mice. The protein expressions of CPT1A, CPT1B, CPT2 and ACOX1 were comparable between the genotypes (Supplementary Fig. 5b), as well as the levels of palmitoyl-carnitine (Supplementary Fig. 5c), indicating that hepatocyte-specific AKAP1 deficiency did not affect FAO. Consistently, fasting serum levels of ketone bodies (acetoacetate (AcAc) and β-hydroxybutyrate (BHB)),

which are markers of hepatic FAO, remained unchanged between the two groups (Supplementary Fig. 5d). Finally, we evaluated the role of hepatic AKAP1 in the regulation of VLDL-TG metabolism. There were no significant differences in ApoB100 and ApoB48 protein expressions in liver tissue between the genotypes (Supplementary Fig. 5e). To further examine this point, we investigated the effect of AKAP1 deficiency on VLDL secretion. Mice were fasted for 6 h and injected with the nonionic surfactant detergent poloxamer 407 (P407). The P407 injection blocks VLDL clearance by inhibiting lipoprotein lipase activity and VLDL lipolysis[17–20]. Blood was collected after P-407 injection and plasma TG were quantified. As shown in Supplementary Fig. 5f, in FFD-fed mice, AKAP1 deficiency did not alter liver VLDL-TG secretion. In combination, these findings suggest hepatocyte-specific AKAP1 deficiency had little effect on fatty acid uptake, β-oxidation and VLDL secretion in FFD-fed mice. Additionally, under HFD, there was a mild increase in VLDL release in AKAP1-HKO mice compared to AKAP1-Flox mice (Supplementary Fig. 5g). This effect may contribute to the relatively mild hepatic steatosis phenotype observed in HFD-fed AKAP1-HKO mice.

Our lipidomics data showed that PE were decreased in liver from AKAP1-HKO mice. To investigate whether PE reduction induced by AKAP1-HKO affect membrane fluidity, the analysis of the PE-to-phosphatidylcholine (PC) ratio (a key determinant of membrane fluidity) and mitochondrial membrane fluidity were conducted across the samples. As illustrated in Supplementary Fig. 5h, i, no significant differences were detected between the two groups. Givern that PE is crucial for the autophagy process, we analyzed key autophagy markers, LC3B-I and LC3B-II, in liver tissue from AKAP1-HKO mice. Compared to the AKAP1-Flox group, liver tissue from AKAP1-HKO mice exhibited a reduced LC3B-II/I ratio, indicative of impaired autophagy (Supplementary Fig. 5j). These data suggest that reduced PE levels and inhibition of autophagy may contribute to the progression of MASH in AKAP1-HKO mice.

Hepatocyte-specific AKAP1 deficiency increases LPA and subsequent TG synthesis by enhancing mitochondrial GPAT activity

To elucidate the molecular mechanism by which AKAP1 regulates triglyceride synthesis, we conducted immunoprecipitation and mass spectrometry analysis (IP-MS) to identify the potential interacting partners of AKAP1. A distinct band of about 80 kDa and 100 kDa was observed in the anti-AKAP1 antibody immunoprecipitation product (Fig. 4a). The target band above 55 kDa was excised and assessed by LC-MS/MS. As shown in Supplementary Fig. 6a, this analysis identified a known AKAP1-binding partner, acyl-CoA synthetase long-chain family member 1 (ACSL1), and a new AKAP1-binding protein, glycerol-3-phosphate acyltransferase (GPAT1). We next confirmed the interaction between AKAP1 and ACSL1 in liver tissue (Supplementary Fig. 6b). Additionally, the interaction between AKAP1 and PKA was also verified (Fig. 4b). ACSL1 was known to catalyze FA to form acyl-CoAs, and direct acyl-CoAs toward oxidation or storage via re-esterification. Our previous study has demonstrated that AKAP1/PKA phosphorylates ACSL1 and inhibits mitochondrial ACS activity[14]. In this study, we also observed an increase in mitochondrial ACS activity in AKAP1-deficient livers, suggesting elevated levels of acyl-CoAs in livers with AKAP1 deficiency (Supplementary Fig. 6c).

Interestingly, the new identified AKAP1-binding protein, GPAT1, has been reported to incorporate acyl-CoAs into TG, diverting them away from oxidation (Supplementary Fig. 6g)[21]. The interaction between GPAT1 and AKAP1 was then validated with co-immunoprecipitation analyses in liver tissue of mice (Fig. 4b). Consistently, significant overlap of intracellular AKAP1 and GPAT1 immunofluorescence signals was observed in palmitic acid and oleic acid (PAOA)-treated AML-12 mouse hepatocytes (Fig. 4c). Knocking out AKAP1 had no effect on the expression levels and subcellular location of GPAT1 (Fig. 4d). However, AKAP1 deficiency significantly reduced
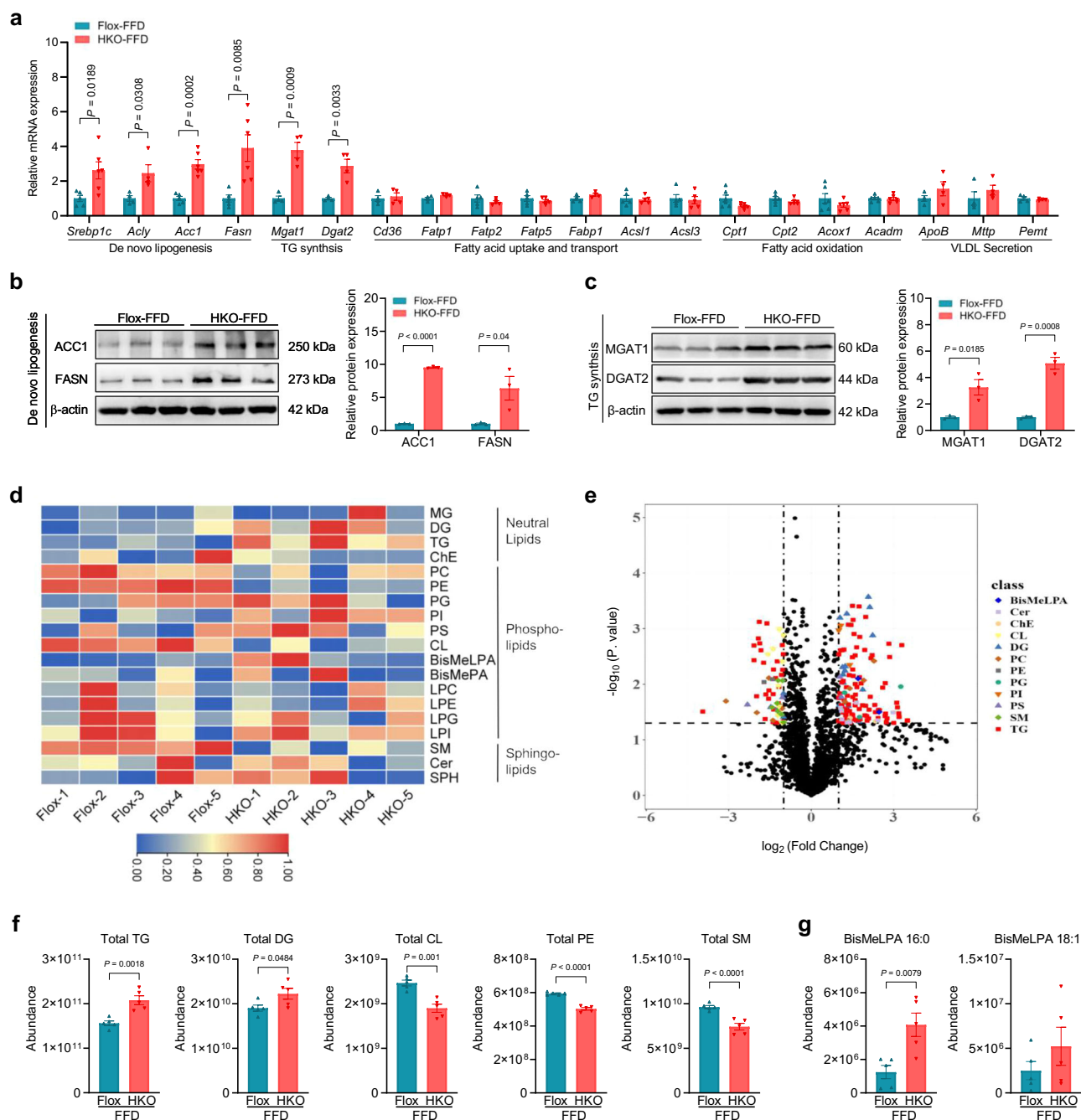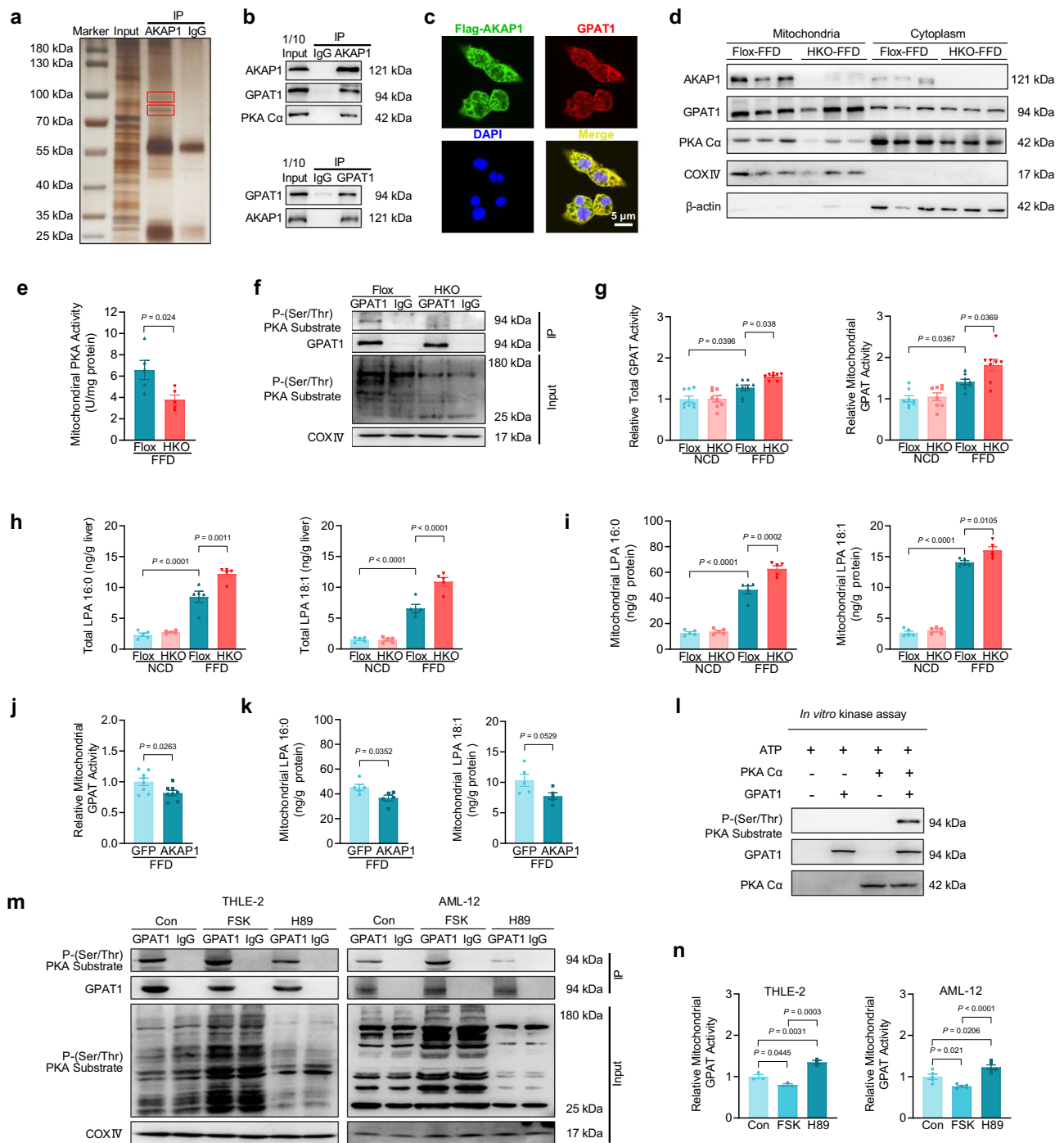
Fig. 3 | Hepatocyte-specific AKAP1 deficiency promotes hepatic steatosis by upregulating TG synthesis. a Relative mRNA expression of lipid metabolism-related genes in the liver tissues from AKAP1-Flox and AKAP1-HKO mice on FFD. $n = 4\text{-}6$ mice per group. For analyze *Srebp1c*, *Acc1*, *Fasn*, $n = 5$ AKAP1-Flox mice and $n = 6$ AKAP1-HKO mice for the FFD group. For analyze *Acly*, *Mgat1*, *Dgat2*, *CD36*, *Fatp1*, *Fabp1*, $n = 4$ mice per group. For analyze *Fatp2*, *Fatp5*, *Acsl1*, *Acsl5*, *ApoB*, *Mttp*, *Pemt*, $n = 5$ mice per group. For analyze *Cpt1*, *Cpt2*, *Acox1*, *Acadm*, $n = 6$ mice per group. **b** Western blotting analysis of proteins involved in de novo lipogenesis (DNL). $n = 3$ mice per group. **c** Western blotting analysis of proteins involved in TG synthesis. $n = 3$ mice per group. β-actin was used as a loading control. **d** Heat maps generated using untargeted lipidomics analysis of hepatic lipid classes in the livers from AKAP1-Flox and AKAP1-HKO mice on FFD. $n = 5$ mice per group. **e** Volcano plot of lipid species [$-\log_{10}$ (P-value) *vs*. $\log_2$ (fold change)] for the comparison AKAP1-HKO *vs* AKAP1-Flox group. The significant difference lipid species were selected by using the criteria of fold changes (FC) ≥ 2 or ≤ 0.5 and P value < 0.05. $n = 5$ mice per group. **f** Abundance of total TG, DG, CL, PE and SM in the livers from AKAP1-Flox and AKAP1-HKO mice on FFD. $n = 5$ mice per group. **g** Abundance of bis-methyl LPA 16:0 (BisMeLPA 16:0) and BisMeLPA 18:1 in the livers from AKAP1-Flox and AKAP1-HKO mice on FFD. $n = 5$ mice per group. Data were expressed as mean ± SEM. Two-tailed Student's *t* test for all data. Source data are provided as Source Data file.

the mitochondrial localization of PKA, whereas the cytoplasmic and total levels of PKA remained unchanged (Fig. 4d and Supplementary Fig. 6d). Additionally, our data revealed a significant decline in mitochondrial PKA activity in AKAP1-HKO mice, while the total PKA activity was unaffected (Fig. 4e and Supplementary Fig. 6e). Given that AKAP1 functions to tether PKA onto mitochondria, it is intriguing to speculate

that AKAP1/PKA may phosphorylate GPAT1 and thus regulate its activity. To demonstrate whether GPAT1 is a phosphorylation target of AKAP1/PKA, GPAT1 was immunoprecipitated from liver mitochondria and its phosphorylation level was analyzed by immunoblotting with anti-phospho-(Ser/Thr) PKA substrates antibody. As indicated in Fig. 4f, the phosphorylation level of GPAT1 was markedly decreased in

Fig. 4 | Hepatocyte-specific AKAP1 deficiency increases LPA and subsequent TG synthesis by enhancing mitochondrial GPAT activity. a IP assay using AKAP1 antibody or IgG. Samples were run on Bis-Tris Gel and then stained with Fast Silver Stain Kit. **b** Co-IP assay showing interaction between AKAP1 and GPAT1 in liver tissue of mice. **c** Representative images of immunofluorescence for Flag-AKAP1 (green), GPAT1 (red) and nuclei (blue) in PAOA treated AML-12 cells infected with Ad-Flag-AKAP1. Scale bar, 5 μm. **d** Western blotting analysis of AKAP1, GPAT1 and PKA Cα protein expression in liver mitochondria and cytoplasm from different groups. *n* = 3 mice per group. COXIV and β-actin were used as mitochondrial and cytosolic loading controls. **e** Mitochondrial PKA activity in liver tissues. *n* = 5 mice per group. **f** Immunoprecipitation of mitochondrial fraction with GPAT1 antibody, blotted for phospho-(Ser/Thr) PKA substrate. **g** Relative total and mitochondrial GPAT activity in liver tissue. *n* = 8 mice per group. **h**–**i** Total LPA (16:0 and 18:1) levels (**h**) and mitochondrial LPA (16:0 and 18:1) levels (**i**) in liver tissue. *n* = 5 mice per group. **j** Relative mitochondrial GPAT activity in liver tissue from AAV8-TBG-

GFP- and AAV8-TBG-AKAP1-treated mice on FFD. *n* = 8 mice per group. **k** Mitochondrial LPA (16:0 and 18:1) levels in liver tissue. *n* = 5 mice per group. **l** The in vitro kinase assay was performed using recombinant GPAT1 protein incubated with or without recombinant PKA Cα protein in the presence of ATP. Phosphorylation was detected using anti-phospho-(Ser/Thr) PKA substrate antibody. **m** Immunoprecipitation of mitochondrial fraction from THLE-2 and AML-12 cells with GPAT1 antibody, blotted for phospho-(Ser/Thr) PKA substrate. **n** Relative mitochondrial GPAT activity in THLE-2 and AML-12 cells following different treatments. Data were from 3 independent experiments in THLE-2 and 4 independent experiments in AML-12. For GPAT activity assay in (**g**, **j** and **n**), palmitoyl-CoA and glycerol-3-phosphate were used as substrates and the production of CoA was monitored using spectrophotometric analysis. All data were expressed as mean ± SEM. One-way ANOVA with Bonferroni post hoc analysis for all data. Source data are provided as Source Data file.

liver from AKAP1-HKO mice when compared with that from AKAP1-Flox controls. The enzyme activities of total GPAT and mitochondrial GPAT were both increased in liver of AKAP1-HKO mice fed with FFD (Fig. 4g and Supplementary Fig. 6f). Consistent with these results, our untargeted lipidomics data also showed that bis-methyl LPA 16:0 (BisMeLPA 16:0, the derivative of LPA 16:0) was significantly elevated in liver of AKAP1-HKO mice fed with FFD (Fig. 3g). Next, we employed the targeted UHPLC-MS/MS quantitative method to analyze the levels of LPA 16:0 and LPA 18:1 in whole cell lysates and mitochondrial fractions. As shown in Fig. 4h, i, both the total and mitochondrial levels of LPA 16:0, as well as the levels of LPA 18:1, were significantly elevated in liver of AKAP1-HKO mice fed with FFD. In contrast, AKAP1 overexpression inhibited mitochondrial GPAT activity and decreased mitochondrial LPA production (Fig. 4j, k). Furthermore, the results of the in vitro kinase assay demonstrated that recombinant PKA Cα directly phosphorylated GPAT1 (Fig. 4l). Meanwhile, GPAT1 phosphorylation and enzyme activity were significantly regulated by the PKA activator FSK and inhibitor H89. An inverse relationship between the enzyme activity and GPAT1 phosphorylation was observed in both THLE-2 human hepatocytes and AML-12 mouse hepatocytes (Fig. 4m, n). Taking together, our findings indicate that AKAP1 acts as a controller to divert acyl-CoAs away from β-oxidation and toward TG synthesis by phosphorylating GPAT1 and inhibiting mitochondrial GPAT activity in liver.

Previous studies have indicated that both AKAP1 and GPAT1 could be phosphorylated by AMPK[22]. However, whether AKAP1 influences AMPK activity and subsequently affects GPAT1 signaling remains unclear. We assessed both the expression and phosphorylation levels of AMPK at Thr172, a critical site for AMPK activation. AKAP1 deficiency did not alter the phosphorylation or expression of AMPK. Neither the knockout nor the overexpression of AKAP1 affected the phosphorylation or expression of AMPK. These findings strongly reduce the likelihood that AKAP1 regulates AMPK (Supplementary Fig. 6h, i).

Phosphorylation of GPAT1 S110 and S611 by PKA inhibits mitochondrial GPAT activity

We then assessed whether GPAT1 is a direct PKA target. Mouse GPAT1 was overexpressed in AML-12 cells incubated with FSK, and then immunoprecipitation was performed with a well-established antibody with high specificity for RRXS^P motifs or GPAT1 antibody (Fig. 5a). RRXS motifs are commonly phosphorylated by PKA. Here, in RRXS^P immunoprecipitated cell lysates, both immunoblotting and MS analysis identified that PKA efficiently phosphorylated GPAT1-RRXS sites (Fig. 5b, c). Sequence analysis of GPAT1 highlighted two potential phosphorylation sites with the motif R/K-R/K-X-S/T including Ser110 and Ser801, which were conserved in mouse, rat and human (Fig. 5d). Moreover, in GPAT1 immunoprecipitated cell lysates, MS analysis identified another phosphopeptide (Fig. 5e) that corresponded to non-RRXS phosphorylation site Ser611, which is also highly conserved (Fig. 5d). We next tested the importance of individual phosphorylation sites on pGPAT1 levels in FSK-stimulated HEK293 cells. As shown in Fig. 5f, FSK markedly increased the phosphorylation of the wild-type GPAT1. However, mutation of either Ser110 or Ser611 to alanine greatly suppressed FSK-stimulated GPAT1 phosphorylation, whereas mutation of Ser801 to alanine did not alter this signal. When all three mutations were present, the signal was virtually completely abolished.

To further determine whether phosphorylation at Ser110 and Ser611 could explain the functional effects of PKA on GPAT activity in hepatocytes, we generated GPAT1^{S110A}/GPAT1^{S611A} and GPAT1^{S110D}/GPAT1^{S611D} mutants to mimic phosphorylation-deficient and constitutively phosphorylated residues, respectively. As shown in Fig. 5g, the S110A/S611A mutations blocked PKA-mediated phosphorylation whereas the S110D/S611D mutations exhibited the opposite effect. Furthermore, the S110A/S611A mutations enhanced mitochondrial GPAT activity, subsequently increased cellular LPA content and TG synthesis. On the contrary, the S110D/S611D mutations led to impaired

GPAT activity, decreased cellular LPA content and reduced TG synthesis (Fig. 5h–k). Taken together, these data indicate that the Ser110 and Ser611 residues of GPAT1 are the phosphorylation sites for PKA, and this phosphorylation can reduce LPA and TG synthesis in hepatocytes.

### Elevated LPA in AKAP1-deficient hepatocytes promoted TNFα production from Kupffer cells

To investigate the role of intracellular LPA in hepatocyte inflammation and to circumvent the binding of extracellularly added LPA to one of its receptors on the plasma membrane, two LPA species (LPA 16:0 and LPA 18:1) were directly introduced into AML-12 mouse hepatocytes using the cationic transfection reagent Lipofectamine 2000 as previously reported[23] (Fig. 6a). As depicted in Fig. 6b, treatment with LPA 16:0 or LPA 18:1 markedly elevated intracellular TG content in AML-12 cells. Meanwhile, the mRNA and protein expressions of ACC1, FASN, MGAT1 and DGAT2 were significantly upregulated in AML-12 cells treated with LPA 16:0 or LPA 18:1 (Fig. 6c, d). These results are consistent with the previously observed upregulation of lipogenesis-related genes at the tissue level following AKAP1 knockout (Fig. 3a–c). Proliferator activated receptor γ (PPARγ) has been shown to be involved in regulation of glucose homeostasis, lipogenesis, and inflammation[24]. Previous study has demonstrated that PPARγ could be activated by intracellular LPA[25]. Therefore, we determined the expression of PPARγ in LPA-treated hepatocytes. The two LPA species markedly induced PPARγ expression in AML-12 cells (Fig. 6c, d). Furthermore, RT-qPCR analysis revealed that treatment with LPA 16:0 or LPA 18:1 significantly upregulated *Tnfα* and *Mcp1* mRNA expression but not *Il1α*, *Il1β*, *Il6* or *Il11* mRNA expression (Fig. 6e). Consistently, hepatocyte TNFα contents and secretions were also increased following treatment with LPA 16:0 or LPA 18:1 (Fig. 6f, g). Meanwhile, hepatocyte injury was induced by these two LPA species as evidenced by heightened levels of ALT and AST in the culture medium (Fig. 6h). These findings indicate that increased endogenous levels of LPAs effectively enhance TG synthesis and induce an inflammatory response in hepatocytes.

Primary mouse hepatocytes (PMH) were isolated from AKAP1-HKO mice and flox littermates and subsequently treated with PAOA. Our data revealed a significant increase in LPA 16:0 in the supernatant derived from AKAP1-HKO hepatocytes compared to AKAP1-Flox hepatocytes (Fig. 6i). Subsequently, primary mouse Kupffer cells (KCs) were incubated with supernatants from AKAP1-HKO and AKAP1-Flox hepatocytes for 12 h, and the inflammatory response in the KCs was assessed. As shown in Fig. 6j, KCs treated with supernatant from AKAP1-HKO hepatocytes exhibited significantly elevated mRNA expression levels of *Tnfα* and *Il1β*, with *Tnfα* showing particularly pronounced upregulation, compared to those treated with supernatant from AKAP1-Flox hepatocytes. Furthermore, TNFα secretion from these KCs was also significantly increased (Fig. 6k). Collectively, these findings suggest that AKAP1 deficiency-induced elevation of LPA 16:0 enhances the secretion of inflammatory factors by KCs, thereby triggering a significant inflammatory response.

Repression of hepatic LPA levels by *GPAM* knockdown ameliorates the exacerbated MASH resulting from AKAP1 deficiency

The interaction between AKAP1 and GPAT1 prompted us to investigate whether AKAP1 deletion-mediated effects were dependent on GPAT1-mediated LPA synthesis. To address this possibility, we knocked down *GPAM* and downregulated hepatic LPA levels in the livers of AKAP1-Flox and AKAP1-HKO mice by intravenous tail injection of adeno-associated virus 8 (AAV8)-expressing sh*GPAM* (Fig. 7a). Western blotting demonstrated that GPAT1 expression was significantly inhibited in livers but not in other tissues in mice treated with AAV8-sh*GPAM* (Fig. 7b, and Supplementary Fig. 7a). AAV8-sh*GPAM* treatment markedly repressed the accumulation of total and mitochondrial LPA in liver tissue of AKAP1-Flox and AKAP1-HKO mice (Fig. 7c, d). Besides, AAV8-sh*GPAM*-treated mice gained less body weight and serum TG
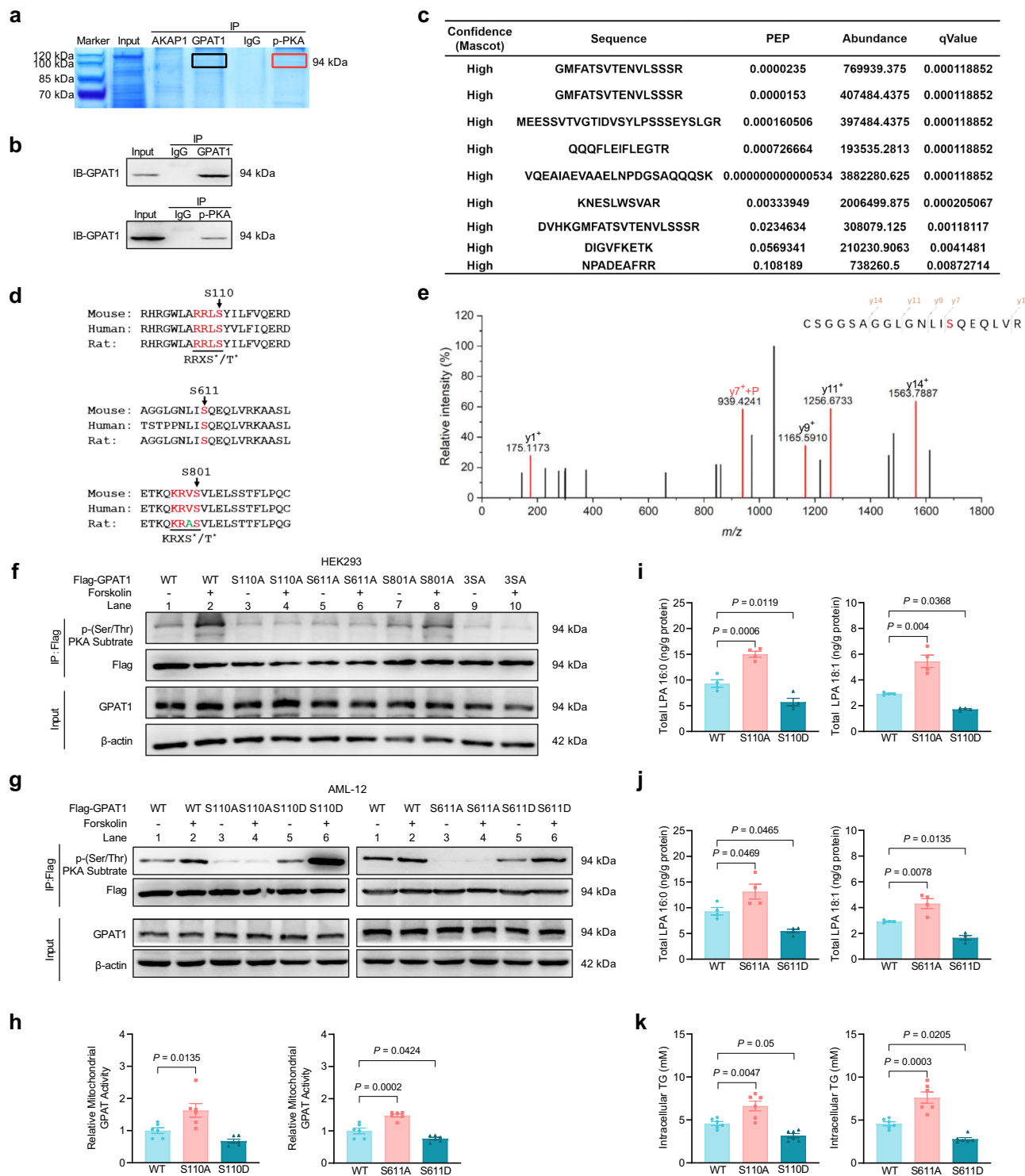
and TC levels when compared with AAV8-sh*NC*-treated mice (Fig. 7e, g). But no significant differences were observed in blood glucose and adipose tissue mass among four groups (Fig. 7f, and Supplementary Fig. 7b). Next, the MASH-like phenotype was evaluated in AKAP1-Flox and AKAP1-HKO mice following AAV8-sh*GPAM* treatment. Along with the decrease in hepatic LPA levels, *GPAT1* knockdown markedly alleviated hepatic steatosis and liver injury, as evidenced by decreased liver weight (Fig. 7h, i), lower NAFLD activity scores (NAS) and Oil Red O positive areas (Fig. 7j, k), reduced hepatic lipid content (Fig. 7n, o), and diminished serum ALT and AST levels (Fig. 7p, q). Notably, these MASH-like phenotypes were also significantly mitigated

in AKAP1-HKO mice by the repression of hepatic LPA through *GPAT1* knockdown. Furthermore, the results of fibrosis severity scores and the infiltration of F4/80-positive inflammatory cells revealed that *GPAT1* knockdown significantly decreased attenuated liver fibrosis and inflammation in AKAP1-HKO mice but not in AKAP1-Flox mice (Fig. 7l, m). These results indicate that inhibition of hepatic LPA levels largely ameliorate the exacerbated MASH resulting from AKAP1 deficiency. Interestingly, although residual GPAT1 protein levels were comparable between the two groups, AKAP1-Flox mice with *GPAT1* knockdown exhibited reduced hepatic steatosis and liver inflammation relative to AKAP1-HKO mice (Fig. 7j–q). We hypothesize that this

Fig. 5 | Phosphorylation of GPAT1 S110 and S611 by PKA inhibits mitochondrial GPAT activity. a Immunoprecipitated GPAT1 and PKA substrates in stable over-expressed GPAT1 AML-12 cells were stained with Coomassie brilliant blue (CBB), 10 μM FSK was added for 30 min before lysis. **b** The immunoprecipitated GPAT1 in (**a**) (black) and immunoprecipitated PKA substrates in (**a**) (red) were blotted with GPAT1 antibody. **c** The major band in (**a**) (red) was cut and digested. GPAT1 peptides were detected by LC-MS/MS. **d** Amino acid sequences of GPAT1 from mouse, human, and rat were aligned. Conserved serine 110 and 801 residues (the motif R/K-R/K-X-S/T) are predicted to be potential PKA phosphorylation sites. **e** The major band in (**a**) (black) was cut and digested. Phosphor-peptides were detected by LC-MS/MS. Only the serine 611 was found to be phosphorylated. **f** HEK293 cells stably expressing Flag-tagged GPAT1 wild-type (WT), S110A mutant, S611A mutant or S801A mutant, followed by IP with an anti-Flag antibody. 10 μM FSK was added 30 min before lysis. Proteins were blotted with an anti-phospho-(Ser/Thr) PKA substrate antibody. This experiment was repeated three times independently.

g AML-12 cells stably expressing Flag-tagged GPAT1 WT, S110A or S110D mutant, S611A or S611D mutant were treated with 10 μM FSK for 30 min, followed by IP with an anti-Flag antibody. Proteins were blotted with an anti-phospho-(Ser/Thr) PKA substrate antibody. This experiment was repeated three times independently. **h** Relative mitochondrial GPAT activity in AML-12 cells stably expressing GPAT1 WT and GPAT1 mutants. In the assay, palmitoyl-CoA and glycerol-3-phosphate were used as substrates and the production of CoA was monitored using spectro-photometric analysis. $n = 6$ biologically independent cells. **i, j** Total LPA 16:0 and LPA 18:1 levels in PAOA treated AML-12 cells stably expressing GPAT1 WT and GPAT1 mutants. $n = 4$ biologically independent cells. **k** Intracellular TG contents in PAOA treated AML-12 cells stably expressing GPAT1 WT and GPAT1 mutants. $n = 6$ biologically independent cells. All data were expressed as mean ± SEM. One-way ANOVA with Bonferroni post hoc analysis for (**h**–**k**). Source data are provided as Source Data file.

difference may arise from the inhibition of residual GPAT1 activity by AKAP1 in AKAP1-Flox mice, a mechanism absents in AKAP1-HKO mice. These supplementary findings further support the conclusion that hepatic AKAP1 deficiency exacerbates diet-induced MASLD by enhancing GPAT1 function.

Hepatic AKAP1 expression is upregulated under metabolic challenge during MASLD pathogenesis

To illustrate the clinical significance of AKAP1 in human MASH, we analyzed the mRNA expression levels of *Akap1* in liver biopsies obtained from 51 metabolic dysfunction-associated steatotic liver (MASL) patients, 155 MASH patients and 10 controls from a large dataset GSE135251. As shown in Fig. 8a, *Akap1* mRNA expression in liver of MASL and MASH patients was significantly upregulated than those in heathy controls. Next, AKAP1 protein expression was measured in liver sections from individuals with healthy livers (normal group), MASL and MASH. Immunohistochemistry analyses showed that AKAP1 protein levels were obviously higher in the liver tissue of patients with MASL and MASH compared with those in healthy liver tissue (Fig. 8b, c). Furthermore, AKAP1 protein level was positively correlated with NAFLD activity scores (NAS) in MASLD (Fig. 8d). Moreover, hepatic AKAP1 expression was significantly increased in mice after 4 weeks of FFD feeding, which persisted to 16 weeks (Fig. 8e–g). To ascertain whether the FFD-induced AKAP1 upregulation is derived from hepatocytes, AKAP1 protein levels were also determined in a hepatocyte model of fatty acid overload using PMH, AML-12 mouse hepatocytes and human hepatic THLE-2 cells incubated with PAOA. As expected, AKAP1 expressions were consistently increased in various hepatocytes after 24 h PAOA treatment (Fig. 8h). Considering that MASLD is often associated with hyperinsulinemia and insulin resistance, AML-12 cells were exposed to either physiologic levels (0.1 nM) or pathologic levels (>1 nM) of insulin. In response to increased dosage and prolonged induction time, we observed a significant upregulation of AKAP1 expression (Fig. 8i). Collectively, these results indicate that AKAP1 expression is significantly increased in livers and hepatocytes after metabolic stimulation, and it is a shared characteristic of human and mouse MASLD.

### GalNAc-siRNA targeting hepatic GPAT1 alleviated diet-induced MASLD in mice

To evaluate the therapeutic potential of targeting GPAT1 for MASH treatment, we employed a hepatocyte-targeted siRNA delivery system, utilizing GalNAc conjugation (This approach involves covalently linking the sense strand of siRNA to GalNAc, which binds specifically to the asialoglycoprotein receptor (ASGPR) on liver cell membranes and has been validated in preclinical studies[26,27]. Subcutaneous injection of GalNAc-si*GPAM* resulted in a specific reduction of GPAT1 expression in the liver (Supplementary Fig. 8a, b). Concurrently, GalNAc-si*GPAM* treatment significantly diminished hepatic steatosis (Supplementary

Fig. 8c, d), reduced liver lipid content (Supplementary Fig. 8g) and decreased serum ALT and AST levels (Supplementary Fig. 8h) in FFD-fed mice. However, *GPAT1* knockdown had no significant impact on liver fibrosis or inflammation (Supplementary Fig. 8e, f), potentially due to the inherently low baseline levels observed in control mice. These findings underscore the therapeutic potential of GPAT1 signaling in the prevention of MASLD.

Discussion

In previous study, we demonstrated that global knockout of AKAP1 in dietary mouse models of obesity resulted in reduced weight, insulin resistance, and fatty liver[14]. However, since the increased energy expenditure in adipose tissue could indirectly reduce liver fat, it was not feasible to determine whether AKAP1 has direct effects on the liver. To address this question, we conditionally deleted AKAP1 from hepatocytes by crossing AKAP1-Flox mice with albumin-cre mice. Surprisingly, in the present study, we found that AKAP1-HKO mice exhibited the increased steatohepatitis upon an FFD. In contrast, restoration of AKAP1 in the liver rescued the exacerbated MASH phenotype in these mice. These data provided compelling evidence establishing a causal role for hepatocyte AKAP1 expression in preventing steatohepatitis in mice. To explore the underlying mechanism of this unexpected finding, we conducted a series of metabolic studies to assess hepatic lipid metabolism. Importantly, we observed a marked elevation in de novo TG synthesis in AKAP1-HKO mice, whereas no significant differences were detected in fatty acid uptake, FAO or hepatic lipid secretion. Further experiments revealed that AKAP1 phosphorylates and inactivates GPAT1 in a PKA-dependent manner, thereby suppressing the conversion of newly synthesized acyl-CoAs into LPA. Notably, AKAP1 deficiency in hepatocytes increased LPA levels, which promoted TG biosynthesis and stimulated KCs to secrete pro-inflammatory cytokines, thus triggering a significant hepatic inflammatory response. Suppression of hepatic LPA levels via *GPAM* knockdown alleviated the exacerbated MASH resulting from AKAP1 deficiency. Collectively, these lines of evidence elucidate a novel role of AKAP1 in TG synthesis and liver inflammation, suggesting that AKAP1/PKA/GPAT1 signalosome-mediated LPA production may be an ideal strategy for MASLD therapy (Fig. 9).

AKAP1 serves as a scaffold protein on the OMM, integrating PKA and other intercellular signal transduction cascades to maintain mitochondrial hemostasis[11]. In brown adipocytes, we have previously reported that AKAP1 inhibits mitochondrial β-oxidation and thermogenesis by interacting with ACSL1[14]. ACSL1 catalyzes the conversion of FA to acyl-CoAs, thereby supplying substrates for the majority of downstream pathways involved in FA metabolism. In adipocytes, ACSL1 specifically directs acyl-CoAs toward β-oxidation[28]. However, in hepatocytes, Li et al. have reported that loss of ACSL1 decreases both TG synthesis and β-oxidation[29]. In the current investigation, we validated that AKAP1 interacted with ACSL1 and exerted a negative
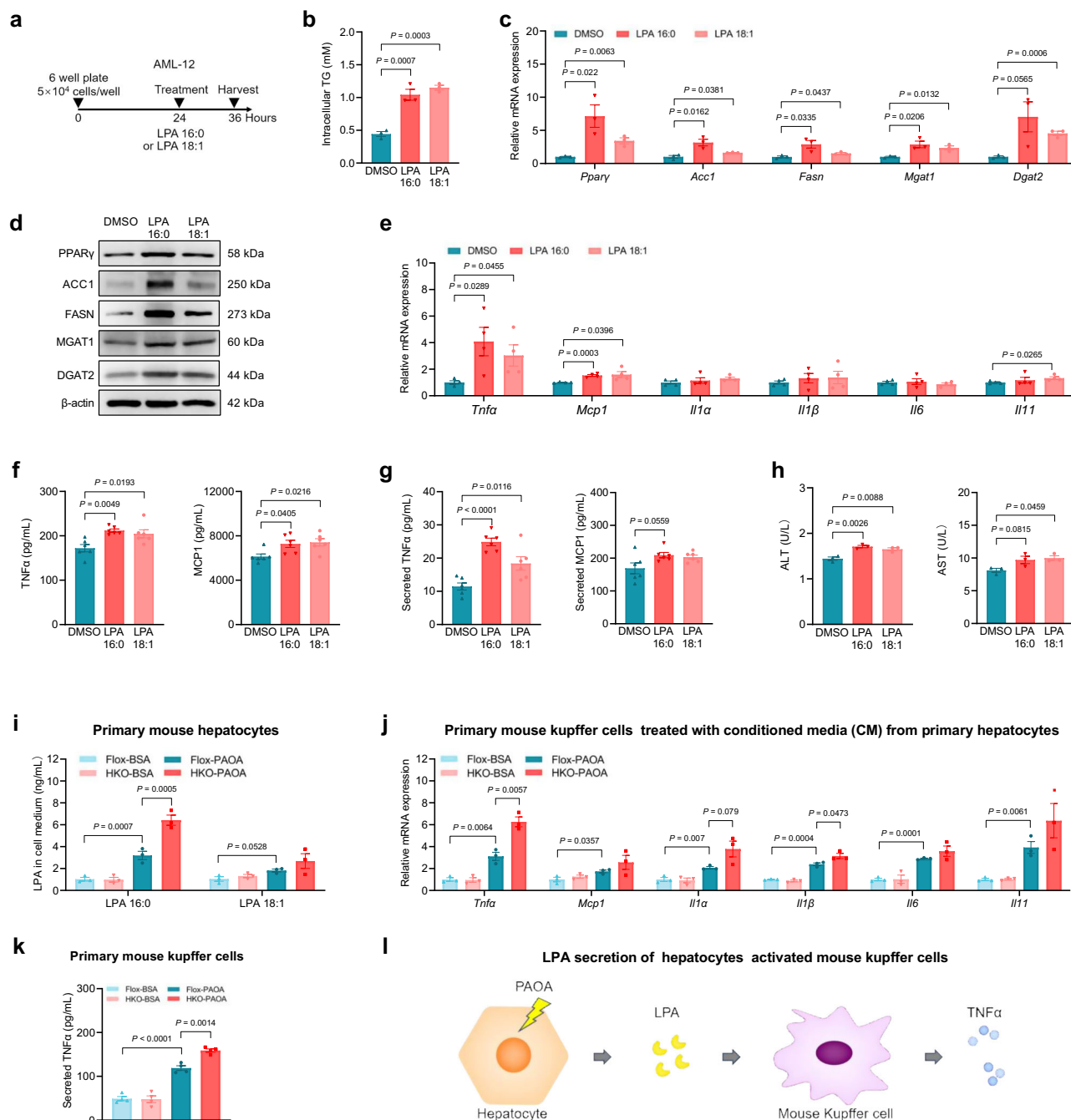
Fig. 6 | LPA enhances TG content in hepatocytes and induces inflammatory response in Kupffer cells. a AML-12 cells were treated with 10 µM LPA 16:0 or 10 µM LPA 18:1 for 12 h. **b** Intracellular TG content in AML-12 cells. $n = 3$ biologically independent cells. **c** Relative mRNA expression levels of *Pparγ*, *Acc1*, *Fasn*, *Mgat1*, *Dgat2* in AML-12 cells. $n = 3$ biologically independent cells. **d** Western blotting analysis of PPARγ, ACC1, FASN, MGAT1, DGAT2 protein expression in AML-12 cells. $n = 3$ biologically independent cells. **e** Relative mRNA expression levels of *Tnfα*, *Mcp1, Il1α, Il1β, Il6* and *Il11* in AML-12 cells. $n = 4$ biologically independent cells. **f** TNFα and MCP1 protein expression in AML-12 cells. $n = 6$ biologically independent cells. **g** TNFα and MCP1 secretions in cell culture supernatant of AML-12 cells. $n = 6$ biologically independent cells. **h** ALT and AST contents in cell culture supernatant
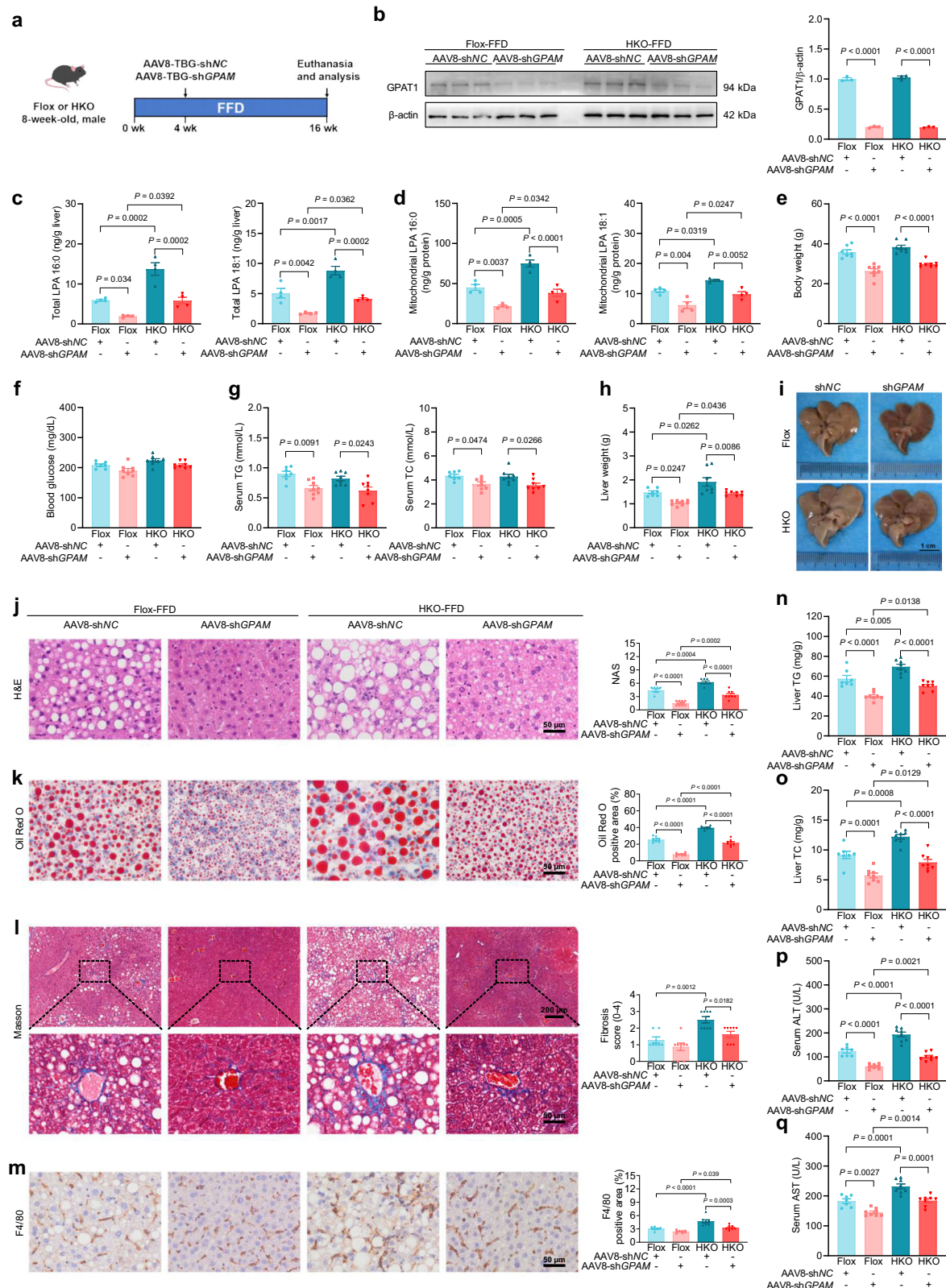
of AML-12 cells. $n = 3$ biologically independent cells. **i** Primary mouse hepatocytes (PMH) isolated from AKAP1-Flox and AKAP1-HKO mice were treated with BSA or PAOA for 24 h, then LPA 16:0 and LPA 18:1 levels were determined in cell culture supernatant. $n = 3$ biologically independent cells. **j** Relative mRNA expression of *Tnfα, Mcp1, Il1α, Il1β, Il6* and *Il11* in mouse KCs treated with conditioned medium (CM) from PMH for 12 h. $n = 3$ biologically independent cells. **k** TNFα secretion in cell culture supernatant of KCs. $n = 4$ biologically independent cells. **l** The release of LPA from PMH activated KCs and increased TNFα secretion. Data were expressed as mean ± SEM. one-way ANOVA with Bonferroni post hoc analysis for all data. Source data are provided as Source Data file.

regulatory effect on mitochondrial ACS activity in the liver. Nevertheless, there was no significant difference in FAO between AKAP1-HKO mice and their controls, as well as in terms of fatty acid uptake and hepatic lipid secretion. Remarkably, de novo TG synthesis was significantly enhanced in AKAP1-HKO mice. This phenomenon

indicates that there are other more critical factors regulating the fate of acyl-CoAs and downstream fatty acid metabolism.

Using IP-MS analysis, we identified GPAT1 as a new interacting partner of AKAP1 in liver tissue. GPAT1, encoded by *GPAM* and located in the OMM, is a member of the GPAT family. GPAT catalyzes the rate-

limiting step in glycerolipid synthesis by combining a fatty acid from an acyl-CoAs with glycerol-3-phosphate to form LPA. In most cells, GPAT1 accounts for approximately 10% of the total GPAT activity, whereas in the liver, it represents 30–50% of the activity[30]. Previous studies have demonstrated that *GPAM* null mice exhibits protection against both diet-induced and genetically driven hepatic steatosis[6,31–33], as well as resistance to hepatic carcinogenic insults[34]. In recent years,

compelling evidence has indicated that mitochondrial GPAT1 variants play a significant role in the predisposition to MASLD in human beings[7–9]. Somatic missense, nonsense, and frameshift mutations of *GPAM* have been identified in biopsy specimens of liver from patients with MASLD and alcohol-related liver disease[8]. A gain-of-function mutation in *GPAM* confers an increased risk of MASLD[9], while a frameshift missense loss-of-function mutation in individuals reduces the

Fig. 7 | Repression of hepatic LPA levels ameliorates the exacerbated MASH resulting from AKAP1 deficiency. a AKAP1-Flox mice and AKAP1-HKO mice (8 weeks of age) were fed on FFD for 4 weeks, followed by intravenous tail injection of AAV8-TBG-sh*GPAM* to specifically knockdown liver *GPAT1* levels. After an additional 12 weeks of FFD feeding, mice were euthanized and analyzed. **b** Western blotting analysis of GPAT1 protein expression from the livers of mice from the indicated groups. *n* = 3 mice per group. β-actin was used as a loading control. **c–d** Total LPA (16:0 and 18:1) levels (**c**) and mitochondrial LPA (16:0 and 18:1) levels (**d**) in liver tissue of mice from the indicated groups. *n* = 4 mice per group. **e** Body weight. **f** Blood glucose levels. **g** Serum TG and TC levels. **h** Liver weight. **i** Representative images of liver dissected from mice in the indicated groups. Scale bar, 1 cm. **j** Representative

H&E-staining images (left) and NAFLD activity score (NAS) of each group (right). Scale bar, 50 μm. **k** Representative Oil Red O staining images (left) and quantification of the Oil Red O positive area (right). Scale bar, 50 μm. **l** Representative Masson's staining images (left) and fibrosis score (right). Upper scale bar, 200 μm; lower scale bar, 50 μm. **m** Representative immunohistochemical staining images of F4/80 (left) and quantification of the F4/80 positive area (right). Scale bar, 50 μm. **n, o** Liver TG and TC levels. **p, q** Serum ALT and AST levels. For (**e–h**) and (**j–q**), *n* = 7 AKAP1-Flox mice injected with AAV8-sh*NC*, and *n* = 8 AKAP1-Flox injected with AAV8-sh*GPAM*, *n* = 8 AKAP1-HKO mice injected with AAV8-sh*NC*, *n* = 8 AKAP1-HKO mice injected with AAV8-sh*GPAM*; Data were expressed as mean ± SEM. One-way ANOVA with Bonferroni post hoc analysis for all data. Source data are provided as Source Data file.

risk of MASLD and correlates with decreased cholesterol levels[7]. These findings highlight the potential for hepatocyte protection against lipotoxicity through modulation of GPAT1 function. In the present study, our findings for the first time revealed that AKAP1 directly interacted with GPAT1 on the OMM and inhibited GPAT activity in hepatocytes. In FFD-fed AKAP1-HKO mice, mitochondrial GPAT activity and LPA content were significantly increased, as well as a significant increase in DNL and TG synthesis. More importantly, the repression of hepatic LPA levels by *GPAM* knockdown significantly inhibited hepatic steatosis in AKAP1-HKO mice. Taking together, these results demonstrate that hepatic AKAP1 deficiency exacerbates diet-induced steatosis by activating GPAT1-mediated LPA production and subsequent TG synthesis. Interestingly, a previous study has demonstrated that endogenous cellular LPA synthesized via GPAT1 can activate PPARγ[25]. Consistent with this study, we found that elevated intracellular LPA significantly increased the expression of PPARγ and DNL-related genes in hepatocytes. Given that hepatic PPARγ functions as a steatogenic-inducer gene activating DNL and lipid droplet accumulation[35–37], it is plausible that the augmented DNL in AKAP1-HKO mice may be partly attributed to the GPAT1/LPA/PPARγ pathway. In AKAP1-HKO mice, hepatic lipid accumulation was more pronounced under FFD than HFD, potentially due to three key factors. Firstly, AKAP1 deficiency enhanced DNL via PPARγ pathway activation without affecting fatty acid uptake. The higher carbohydrate content, particularly fructose, in FFD likely amplified this effect, leading to increased DNL flux and TG synthesis. Secondly, AKAP1-HKO mice exhibited slightly elevated VLDL release under HFD conditions compared to AKAP1-Flox mice. Thirdly, baseline hepatic TG levels in AKAP1-Flox mice were significantly higher under HFD than FFD, under these conditions, the capacity for further TG accumulation due to AKAP1 knockout may have already approached its limit.

LPA has long been known as an important bioactive lipid and an inflammatory mediator[38]. In vertebrates, significant amounts of LPA can be detected in various biological fluids. Extracellular LPA can induce cell inflammation via G-protein coupled receptors (LPAR1-6), which are widely distributed across various tissues[39]. A recent study has shown that exogenous LPA promotes the inflammatory response in KCs, and an i.p. injection of LPA also has significant effects on inflammation in mice[40]. In addition, LPA can be converted into phosphatidic acid by 1-acyl-sn-glycerol-3-phosphate-acyltransferase-2 (AGPAT2). Another study has demonstrated that knockdown of *AGPAT2* in the liver and white adipose tissue (WAT), using an antisense oligonucleotide, led to accumulation of LPA in the liver and WAT, which is associated with lipodystrophy and inflammation in these tissues[41]. These findings suggest that intracellular LPA may be an early metabolic trigger for tissue inflammation. In this study, we observed a significant increase in both LPA 16:0 and LPA 18:1 levels in AKAP1-HKO mice following an FFD. Then LPA 16:0 and LPA 18:1 were directly introduced into hepatocytes. Consistent with previous studies, both LPA 16:0 and LPA 18:1 treatment significantly increased intracellular TG content and inflammation response in hepatocytes. Moreover, LPA specifically augmented the TNFα content and secretion in hepatocytes, leading to increased hepatocyte injury. Notably, AKAP1

deficiency-driven upregulation of LPA production enhances the secretion of pro-inflammatory factors by KCs, consequently initiating a pronounced inflammatory response. Furthermore, liver fibrosis and inflammation, as well as the levels of serum biomarkers of liver injury, were significantly rescued in FFD-fed AKAP1-HKO mice by intravenous tail injection of AAV8-sh*GPAM*. These results indicate that GPAT-derived LPA induces hepatocyte inflammation and contributes to the pathogenesis of MASH.

PE is a key component of cell membranes. The PE-to-PC ratio is widely regarded as a key determinant of membrane fluidity[42,43], which, in turn, significantly influences various membrane-associated processes, including signal transduction, membrane protein function, vesicular transport, and others. In addition, PE covalently conjugates with LC3 in a process known as LC3-PE lipidation, leading to the formation of lipidated LC3 (LC3-II), a key marker of autophagosome formation[44]. In the present study, we found that AKAP1 deficiency did not affect mitochondrial membrane fluidity, but exhibited a reduced LC3B-II/I ratio, indicating impaired autophagy in the liver. These data suggest that reduced PE levels may contribute to the progression of MASH in AKAP1-HKO mice, however, further studies are needed to fully elucidate these mechanisms.

The AKAP family primarily functions by anchoring PKA to specific subcellular locations through its interaction with the regulatory (R) subunit of PKA, with AKAP1 being the only member specifically localized to mitochondria. Our data demonstrated that knockout of AKAP1 did not regulate the global expression or activity of PKA but significantly diminished the expression and activity of mitochondrial PKA. Furthermore, knockout of AKAP1 had no effect on the mitochondrial localization of GPAT1, however, it significantly decreased the phosphorylation level of GPAT1 and enhanced both mitochondrial and total GPAT activity in a PKA-dependent manner in hepatocytes. Previous studies have shown that the activity of GPAT1 is post-transcriptionally regulated through a phosphorylation mechanism[45,46]. Using rat liver mitochondria, Onorato et al. have found that the activity of GPAT1 in cell-free systems is affected by casein kinase-2, but the site and significance of the modification is unknown[46]. In primary rat hepatocytes, AMP-activated protein kinase (AMPK) phosphorylates and inhibits GPAT1[47], however, chronic AMPK activation does not decrease GPAT1 activity in rats[48]. Hence, the regulatory mechanism of GPAT1 in hepatocytes remains elusive. In the present study, we found that GPAT1 was a downstream target of PKA. The Ser110 and Ser611 residues of GPAT1 were identified as the primary phosphorylation sites for PKA, and this post-translational modification was found to attenuate the synthesis of LPA and TG in hepatocytes. Given that AKAP1 serves as the scaffold protein anchoring PKA to mitochondria, we propose that AKAP1 may act as a platform for assembling PKA and GPAT1 into a "signalosome", which finely modulates GPAT1 activity and governs mitochondrial LPA production. Considering the broad substrate spectrum of PKA and its complex roles in metabolic regulation and cell fate determination[49,50], targeting mitochondrial PKA, as opposed to globally modulating total hepatic PKA, may provide a more precise intervention strategy with fewer side effects.
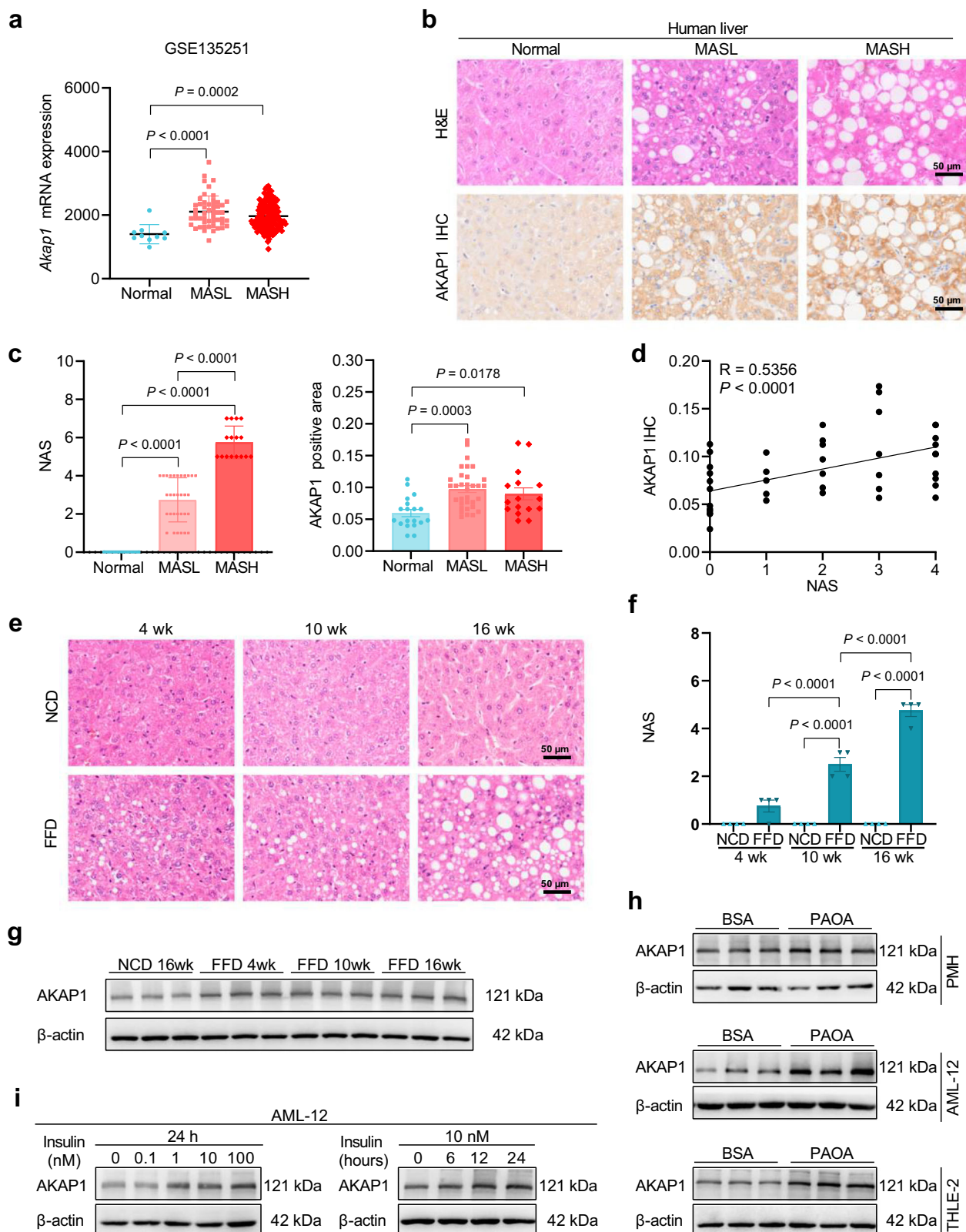
In this study, AKAP1 expression was significantly upregulated in human liver tissues under MASL and MASH. It is well known that MASLD is often associated with hyperlipidemia, hyperinsulinemia and insulin resistance. Our data showed that both high concentrations of PAOA and insulin markedly upregulated AKAP1 protein expression in hepatocytes, indicating an increase of AKAP1 levels in hepatocytes following metabolic stimuli. We propose the increase of AKAP1 with

MASLD as a compensatory mechanism, which may restrict the progress of MASLD through compensating for TG synthesis and hepatic inflammation. In FFD-fed AKAP1-Flox mice, we observed that overexpression of hepatic AKAP1 significantly alleviated hepatic steatosis and hepatocellular injury, indicating that enhancing hepatic AKAP1 expression could serve as a protective measure against MASLD. Consistently, treatment with GalNAc-si*GPAM* effectively reduced hepatic

Fig. 8 | Hepatic AKAP1 expression is increased in MASLD pathogenesis.
a Comparison of liver *Akap1* mRNA expression between normal controls ($n = 10$) and patients with MASL ($n = 51$) and MASH ($n = 155$) in the GEO database GSE135251. **b** Representative images of H&E (upper) and AKAP1 immunohistochemical staining (lower) in liver sections from individuals with MASL ($n = 31$), MASH ($n = 16$) and normal controls ($n = 19$). Scale bar, 50 μm. **c** NAFLD activity score (NAS) and AKAP1 positive area analysis of liver section of normal controls ($n = 19$), MASL ($n = 31$) and MASH ($n = 16$) human subjects. **d** Correlation of AKAP1 protein levels and NAFLD activity score (NAS) in patients with MASLD and healthy controls determined by Pearson correlation analysis ($R = 0.5356$, $P < 0.0001$). **e** Representative H&E-staining images in liver sections from mice fed an NCD or FFD for 4 weeks, 10 weeks and 16 weeks. $n = 4$ mice per group. Scale bar, 50 μm. **f** NAFLD activity score (NAS) of

each group. $n = 4$ mice per group. **g** Western blotting analysis of AKAP1 protein expression in liver extracts from mice fed an NCD or FFD for 4 weeks, 10 weeks and 16 weeks. $n = 3$ mice per group. **h** Western blotting analysis of AKAP1 protein expression in PMH, AML-12 and THLE-2 cells treated with PAOA or BSA for 24 h, data were from three independent experiments. **i** Western blotting analysis of AKAP1 protein expression in AML-12 cells stimulated with insulin at indicated concentrations for 24 h (left) or at 10 nM for indicated times (right), data were from three independent experiments. β-actin was used as a loading control. All data were expressed as mean ± SEM. One-way ANOVA with Bonferroni post hoc analysis for (**a**, **c** and **f**); Spearman's rank correlation coefficient analysis for (**d**). Source data are provided as Source Data file.
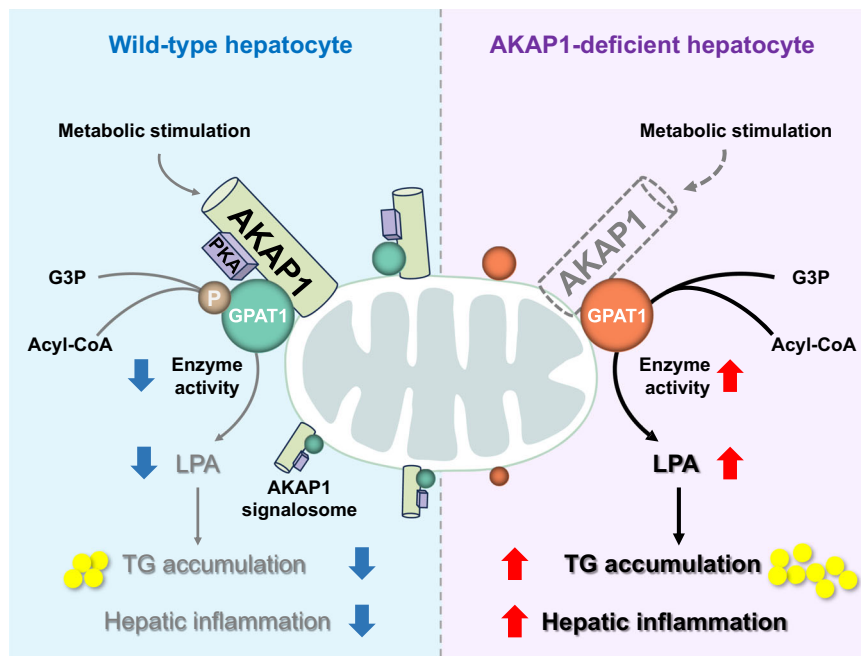
Fig. 9 | Hepatocyte-specific AKAP1 deficiency exacerbated hepatic steatosis and steatohepatitis in mice. Mechanistically, AKAP1 phosphorylates and inactivates glycerol-3-phosphate acyltransferase 1 (GPAT1) in a PKA-dependent manner. AKAP1 deficiency enhances GPAT1 activity increased lysophosphatidic acid (LPA) production and decreases subsequent TG synthesis and hepatic inflammation by enhancing GPAT1-mediated Lysophosphatidic Acid Synthesis.

GPAT1 levels, resulting in decreased hepatic lipid accumulation and liver injury in FFD mice. Collectively, these findings underscore the therapeutic potential of AKAP1/GPAT1 signaling in the treatment and prevention of MASLD.

In conclusion, our study showed that AKAP1 protected against MASLD progression. Hepatocyte-specific knockout of AKAP1 significantly enhanced GPAT1-derived LPA contents, increased subsequent TG synthesis and liver inflammation in response to metabolic stress. Mechanistically, AKAP1/PKA directly interacted with GPAT1, phosphorylated and inhibited GPAT1 activity, and eventually reduced intracellular LPA. Repression of intracellular LPA levels by *GPAM* knockdown alleviated the MASH phenotype resulting from AKAP1 deficiency. Our study highlights the precise regulation of mitochondrial AKAP1 over newly formed acyl-CoAs, indicating that AKAP1/GPAT1 signalosome-mediated LPA production may represent an optimal strategy for MASLD therapy.

Methods
Ethics statement
The experiments using human samples were approved by the research ethics committee of Xijing Hospital, Fourth Military Medical University, Xi'an, P.R. China and all donors provided written informed consent (Permission Number: KY20213448-1). All animal experiments were conducted according to the guidelines of the Institutional Animal

Care and Use Committee of the Fourth Military Medical University (Permission Number: IACUC-20220351).

Human liver samples
Human liver samples were obtained from 66 patients undergoing hepatic surgery due to hepatic hemangioma or cyst at the Xijing Hospital (Xi'an, China). Two blinded experienced pathologists independently used the Nonalcoholic Steatohepatitis Clinical Research Network (NASH-CRN) scoring system to evaluate the NAFLD activity score (NAS). The normal samples possessed an NAS of 0. The MASH samples possessed an NAS > 4, or NAS at 3–4 but exhibiting fibrosis. The clinical characteristics of these subjects are provided in Supplementary Table 1. Exclusion criteria of the study included excessive alcohol consumption (>140 g for men or >70 g for women, per week), drug abuse, autoimmune hepatitis, or viral infection (for example, infection with hepatitis B virus or hepatitis C virus).

Diet-induced MASLD and MASH model
In this study, only male mice were used since MASLD is a sex dimorphic disease and estrogen has been shown to be a key factor in MASLD[51]. Male C57BL/6J mice (8 weeks of age) were housed under a 12 h light-dark cycle with a room temperature (22 ± 0.5 °C) in a specific pathogen free animal center at Fourth Military University. Mice had free access to water and food unless otherwise stated. To establish a MASLD model,

mice were fed a high-fat diet (HFD; 20 kcal% protein, 60 kcal% fat, and 20 kcal% carbohydrate; D12492; Research Diets) for 24 weeks. To establish a MASH model, mice were fed a fast-food diet (FFD; 17 kcal% protein, 40 kcal% fat, 43 kcal% carbohydrate and 0.2% cholesterol (D12079B; Research Diets) together with a total of 42 g/L of carbohydrate mixed in drinking water at a ratio of 45% glucose and 55% fructose by weight) for 16 weeks as previously reported[52–54]. The corresponding control group mice were fed a normal chow diet (NCD, Jiangsu-Xietong, Inc., Nanjing, China).

Construction of hepatocyte-specific *AKAP1* knockout mice
AKAP1-Flox (AKAP1$^{flox/flox}$) mice on the C57BL/6 background were generated by inserting loxP sequences encompassing the exon 2 of the AKAP1 gene using homogenous recombination by Shanghai Model Organisms (Shanghai, China). Mice with hepatocyte-specific knockout of AKAP1 (AKAP1-HKO) were created by crossing AKAP1-Flox mice with Alb-Cre transgenic mice. The genotyping PCR was performed using genomic DNA extracted from the tail by One Step Mouse Genotyping Kit (PD101-01; Vazyme). The primers 5′- AGACGCTGGAGATCC TGCTTGAAT -3′ and 5′- CAGACCAAAGCTGCTGATCACA -3′ for AKAP1 loxP1; 5′- TGCTGCCCATCCCTGTGTTATCC -3′ and 5′- CTGCGGCTGT CCTGGGTGAA -3′ for AKAP1 loxP2; and 5′- AGACGCTG GAGATCCTGCTTGAAT -3′ and 5′- CTGCGGCTGTCCTGGGTGAA -3′ for Cre recombinase were used as suggested by Shanghai Model Organisms.

Adeno-associated virus injection
AAV8-TBG-Flag-AKAP1 virus carrying mouse AKAP1 with a liver specific promoter TBG was generated by Hanbio Biotechnology Co., Ltd. (Shanghai, China), and AAV8-TBG-GFP was used as a negative control. To restore hepatocyte-specific AKAP1 expression in AKAP1-HKO mice, the male 8-week-old mice were placed on FFD for 4 weeks and then injected with 200 μL AAV8-TBG-Flag-AKAP1 (5×10^{11} vector genomes (Vg) /mouse) via the tail vein. After another 12 weeks of FFD feeding, the mice were sacrificed for analysis. To knockdown *GPAT1* in the liver, mice were injected with AAV8-TBG-sh*GPAM* (5×10^{11} Vg /mouse, Genomeditech (Shanghai) Co., Ltd). The target sequence of shRNA for *GPAM* was 5′ CCGAATGATGTTGCTGATGAA-3′.

GalNAc-conjugated siRNA delivery
GalNAc-conjugated siRNA delivery in vivo was conducted as previously reported[55]. Si*GPAM* and si*NC* conjugated to N-acetylglucosamine (GalNAc) were purchased from GenePharma Co., Ltd (Shanghai, China) and subsequently diluted with PBS. To achieve hepatocyte-targeted siRNA delivery, 8-week-old male C57BL/6J mice were fed FFD for 8 weeks. Subsequently, the animals were divided into two groups and subcutaneously injected with 10 mg/kg of GalNAc-si*GPAM* or GalNAc-si*NC* every two weeks for additional 8 weeks, while continuing the same diet. A total of five injections were administrated. Mice were euthanized and analyzed three days after the final injection. The target sequence of siRNA for GPAM was 5′ CCGAATGATGTTGCTGATGAA-3′.

Cell lines culture and treatment
The AML-12 (mouse liver cell line), HEK293T and HEK293 were purchased from the Cell Bank of the Type Culture Collection of the Chinese Academy of Sciences (Shanghai, China). THLE-2 (human liver cell line) were purchased from Xuanya Biotechnology Co., Ltd. (Shanghai, China). AML-12 cells were cultured in AML-12 cell-specific culture medium (Hycyte™, TCM-G709, DMEM/F12 medium supplemented with 10% FBS, 1% ITS, 40 ng/mL dexamethasone and 1% penicillin/streptomycin). HEK293T, HEK293, and THLE-2 were cultured in DMEM supplemented with 10% FBS and 1% penicillin/streptomycin. Cells were cultured in a humidified atmosphere of 5% CO_2 at 37 °C. No commonly misidentified cell line was used in this study. All the cell lines were routinely tested negative for mycoplasma contamination. To establish a MASLD model in vitro, AML-12 cells and THLE-2 cells were treated with 0.5 mM palmitic acid (PA; P0500; Sigma-Aldrich) and 1.0 mM oleic acid (OA; O-1008; Sigma-Aldrich) for 24 h.

LPA treatment
AML-12 cells were treated with LPA as previously described[56]. 5×10^4 AML-12 cells were seeded per well of a 6-well plate. After 24 h, the medium was changed to serum-free medium, and cells were transfected with 10 μM LPA 16:0 or 10 μM LPA 18:1 in total volume of 2 mL medium with 10 μL Lipofectamine 2000 (Thermo Scientific), following manufacturer's protocol.

Adenovirus infection
Adenoviruses containing the sequences of mouse AKAP1 (Ad-Flag-AKAP1) and ad-green fluorescent protein (Ad-GFP) were produced by Hanbio Biotechnology Co., Ltd. (Shanghai, China). The titer of adenovirus was 1×10^{10} plaque forming units (PFU)/mL. For AKAP1 overexpression, AML-12 cells were infected with Ad-Flag-AKAP1 (MOI = 100) for 48 h. After adenovirus infection, the AML-12 cells were subjected to PAOA for 24 h.

Isolation, culture, and treatment of primary hepatocytes and Kupffer cells from mouse livers
Primary mouse hepatocytes (PMH) were isolated from 6- to 8-week-old male AKAP1-Flox and AKAP1-HKO mice. Liver perfusion was performed following a standard two-step perfusion method. Briefly, mice were anesthetized and then perfused through the portal vein with perfusion medium consisting of Ca^{2+}-free Hank's balanced saline solution (HBSS), 0.5 mM EDTA and 25 mM HEPES, followed by liver digest medium containing HBSS with Ca^{2+}-Mg^{2+} containing 0.05% Collagenase Type IV (Gibco) and 25 mM HEPES. Next, the liver was removed and gently teased apart in ice-cold DMEM and filtered through a 70 μm cell strainer. The cell suspension was centrifuged at 50 g for 5 min at 4 °C to separate hepatocytes and nonparenchymal cells (NPCs). For hepatocyte isolation, the precipitate was washed three times with ice-cold DMEM at 50 g for 5 min at 4 °C. and were cultured in DMEM with 10% fetal bovine serum (FBS), 1% penicillin/streptomycin at 37 °C in a humidified atmosphere with 5% CO_2 on collagen-I-coated plates.

Primary Kupffer cells (KCs) were isolated from 6-8-week-old male C57BL/6 mice. The isolation procedure was adapted from a previously published method with modifications[57,58]. After the two-step perfusion, NPCs were separated through density gradient isolation with OptiPrep (Sigma Aldrich, #D1556) as follows: (1) NPCs were centrifuged at $650 \times g$ for 10 min at 4 °C; (2) The pellet of NPCs was resuspended in 5 mL of 17.6% OptiPrep solution. Then, 5 mL of 8.2% OptiPrep solution and 2 mL of B-PBS (PBS + 0.1% BSA) were carefully layered on top of the cell suspension; (3) The OptiPrep gradient was centrifuged at $1400 \times g$ for 30 min without braking at room temperature (RT). This step allows the isolation of a mixed suspension (cell fraction between the interface of 8.2% and 17.6% OptiPrep) of liver sinusoidal endothelial cells (LSECs) and KCs. KCs adhere rapidly to cell culture dishes, whereas LSECs do not. This adherence property was used to separate KCs from LSECs. Thus, KCs/LSECs were resuspended in DMEM medium and incubated at 37 °C for 30 min. The supernatant containing LSECs was aspirated, and the dish was washed with DPBS. The adherent KCs were digested with trypsin, counted, and plated in collagen-coated 24-well plates at a concentration of $5-6 \times 10^5$ cells/mL in complete DMEM medium.

PMH from AKAP1-Flox and AKAP1-HKO were treated with BSA or PAOA for 24 h. After this incubation period, the conditioned medium (CM) was collected and filtered through a 0.22 μm filter. Subsequently, KCs were treated with the CM obtained from BSA- or PAOA-treated PMH for an additional 12 h. After this treatment, both the KCs and the cell medium supernatant were collected for further analysis.

Lentivirus production and infection

For the GPAT1 overexpression plasmid (pLVX-CMV-Flag-GPAT1), the coding sequence (CDS) of GPAT1 from mouse cDNA was amplified by PCR and cloned into a pLVX-CMV plasmid (Clontech, 632164). A Fast Site-Directed Mutagenesis kit (TIANGEN, KM101) was used to generate mutant versions of GPAT1 using wild-type GPAT1 (pLVX-CMV-Flag-GPAT1) as the template. All plasmids were verified by Sanger sequencing. The primers used to generate these plasmids are listed in Supplementary Table 2. To generate lentivirus, the pLVX-GPAT1 and pLVX-GPAT1 mutants were co-transfected with psPAX2 and pMD2.G into HEK293T cells using polyethylenimine linear (PEI) (Yeasen, Shanghai, China). The cells were incubated at 37 °C, 5% CO_2 for 48 and 72 h, then the medium containing lentiviral particles were harvested, passed through a 0.45 μm filter and infected target cells. For lentiviral infection, HEK293 cells and AML-12 cells were cultured in basal medium until 70% confluence and then infected with indicated lentivirus-containing medium for overnight in the presence of 5 μg/mL polybrene. Expression levels of GPAT1 in these puromycin-selected cells were analyzed using Western blotting.

Mouse metabolic and liver function assays

Body weight was assessed in mice every two weeks. For glucose tolerance tests (GTT) and insulin tolerance tests (ITT), mice were fasted for 6 h (08:00–14:00) and then intraperitoneally injected with a D-glucose solution in saline (1 g/kg body weight) and insulin solution in saline (0.75 U/kg body weight), respectively. Blood was taken from the tail vein to measure the glucose concentration at 0, 15, 30, 60, 90, and 120 min after injection using blood glucose test strips and a glucometer (Roche, USA). The areas under the curve (AUC) were calculated using the conventional trapezoid rule. Blood samples were obtained after 6 h fast, the fasting blood glucose levels were measured using a glucometer (Roche, USA). Serum triglyceride (TG), total cholesterol (TC), alanine aminotransferase (ALT) and aspartate aminotransferase (AST) concentrations were measured with an automatic biochemical analyzer (7170, Hitachi, Tokyo, Japan).

Hepatic triglyceride and cholesterol assay

Commercial kits were used to measure the contents of total TG and TC in the liver according to the manufacturer's instructions (290-63701 for TG, 94-65801 for TC, Wako, Tokyo, Japan). The final level of TG and TC were normalized with liver tissue weight.

Histological analyses

Liver sections were embedded in paraffin and then stained with hematoxylin-eosin (H&E). OCT-embedded liver sections were used for Oil Red O (O0625; Sigma-Aldrich; St. Louis, MO, USA) staining. Masson's Trichrome staining (G1006, Servicebio, Wuhan, China) was used to assess fibrosis severity. The histological features of the tissues were captured using a slide scanner (Olympus research slide scanner VS200). The severity of liver steatosis, inflammation and fibrosis was assessed by peers blindly. The NAS (0–8) consists of liver steatosis (scale of 0–3), lobular inflammation (scale of 0–3), hepatocellular ballooning (scale of 0–2). Fibrosis score was defined by Kleiner et al.[59,60], based on positive staining across the whole liver section. Fibrosis was staged (0–4): 0 = no fibrosis; 1a = mild zone 3 perisinusoidal fibrosis; 1b = moderate zone 3 perisinusoidal fibrosis; 1c = portal/periportal fibrosis only; 2 = zone 3 and portal/periportal fibrosis; 3 = bridging fibrosis; 4 = cirrhosis.

Immunohistochemistry (IHC)

Paraffin embedded tissue slides were deparaffinized and subjected to antigen retrieval in citric acid buffer. Slides were incubated with 3% hydrogen peroxide and blocking buffer for 5 min and 30 min respectively then primary antibody [anti-AKAP1 (1:200, NOVUS); anti-F4/80 (1:1000, Servicebio), α-SMA (1:500, Servicebio)] overnight at 4 °C.

Following wash with PBS, biotin conjugated secondary antibody and streptavidin conjugated tertiary antibody was added. Finally, positive signals were detected with 3,3'-diaminobenzidine (DAB) solution. Images were captured using a slide scanner (Olympus research slide scanner VS200).

Immunofluorescence

Frozen liver sections were incubated with anti-F4/80 antibody (1:200, Servicebio Technology, China) at 4 °C overnight, followed by 1 h incubation with a fluorophore-conjugated secondary antibody (Alex Flour 568 goat anti-Rabbit IgG (H + L); A11036; Invitrogen; Carlsbad, CA, USA) at room temperature. For coverslip staining, AML-12 cells infected with Ad-Flag-AKAP1 were incubated with mouse anti-Flag (1:1000, Sigma-Aldrich, China) and rabbit anti-GPAT1 (1:100, Abclonal Technology, China) at 4 °C overnight and then labeled with the corresponding secondary antibody for 1 h at room temperature. Finally, samples were stained with DAPI at room temperature for 20 min. Images were obtained using Olympus FV3000 laser-scanning confocal microscope (Tokyo, Japan).

Cellular TG, ALT and AST assay

Intracellular TG levels were measured using a commercial kit (E1013-105, Applygen Technologies Inc., Beijing, China). The levels of ALT and AST in cell culture medium were measured using the ALT and AST (C009-2-1for ALT, C010-2-1 for AST; NjjcBio) assay kits.

Inflammatory cytokines assay

The concentrations of mice inflammatory cytokines, TNFα and MCP1 in cells and from cell culture supernatant were quantified by TNFα ELISA Kit (CSB-E04741m, Cusbio) and Mouse MCP1/MCAF ELISA Kit (CSB-E07430m, Cusbio) following the manufacture's protocol.

RNA isolation and Quantitative RT-PCR

Total RNA from tissues or cells was extracted using Total RNA Kit I (Omega). 1000 ng total RNA was reverse transcribed to generate cDNA using PrimeScipt™ RT Reagent Kit with gDNA Eraser (Takara, Japan). Standards were used to create a standard curve. Quantitative real-time PCR (qRT-PCR) was performed on CFX 96™ Real-Time System (Bio-Rad, USA) using TB Green® Premix Ex Taq™ Kit (Takara, Japan) with specific primers as listed in Supplementary Data 1. Relative gene expression was calculated using the $2^{-\Delta\Delta Ct}$ method from at least three independent experiments after being normalized to β-actin.

Isolation of Mitochondria and plasma membrane

Mitochondria were isolated from fresh livers using Tissue Mitochondria Isolation Kit (Beyotime, C3606) and from cells using Cell Mitochondria Isolation Kit (Beyotime, C3601). The plasma membrane was extracted using Membrane and Cytosol Protein Extraction Kit (Beyotime, P0033) according to the manufacturer's protocol.

Western blotting

Cells and tissues were homogenized in RIPA lysis buffer (P0013B, Beyotime, Shanghai, China) supplemented with PMSF, complete protease inhibitors (Roche) and phosphorylase inhibitor (Roche). For Western blotting analysis of liver AKAP1, fresh liver tissue was harvested and homogenized immediately to avoid protein degradation. Protein concentration was determined using the BCA Assay Kit (P0011, Beyotime, Shanghai, China). Then, equal quantities of the indicated protein were separated by 10% SDS-PAGE gels and transferred to polyvinylidene difluoride PVDF membranes (Millipore). The membrane was blocked with 5% skim milk in Tris-buffered saline (TBST) and then incubated with the indicated primary antibodies at 4 °C overnight. After 1 h incubation with HRP-conjugated secondary antibodies, proteins bands were visualized by a chemiluminescence system

(ChemiScope 6100) and quantified by ImageJ software (NIH, Bethesda, MD). All antibodies used were listed Supplementary Data 2.

Co-immunoprecipitation (Co-IP) and mass spectrometric (MS) analysis

Pierce™ Classic Magnetic IP/Co-IP Kit (Thermo Fisher Scientific, USA) was used for immunoprecipitation (IP). Fresh liver tissue, cells or isolated liver mitochondria were lysed with IP lysis buffer. 1 mg of protein was immunoprecipitated with indicated primary antibody overnight at 4 °C. Subsequently, 20–40 µL of fully suspended protein A/G magnetic beads were added and incubated at room temperature for 2 h. Then, the beads were washed three times with Wash Buffer and resuspended and boiled in loading buffer. The supernatant was further electrophoresed through SDS-PAGE and stained with silver or Coomassie brilliant blue (CBB). Stained protein bands were dispatched to Applied Protein Technology Co., Ltd. (Shanghai, China) for LC-MS/MS analysis. The analysis was conducted on a Q Exactive mass spectrometer coupled to Easy nLC (Thermo Fisher Scientific) using a routine method. MS data were acquired using a data-dependent top10 method dynamically choosing the most abundant precursor ions from the survey scan (300–1800/mz) for higher energy collisional dissociation (HCD) fragmentation. The data of MS were analyzed by MaxQuant software. Spectra data were searched against a UniProt mouse database (www.uniprot.org).

In vitro kinase assay

The in vitro kinase assay was conducted as previously described[61]. Recombinant GPAT1 (Cat No. Ag3120) and PKA Cα (Cat No. Ag21478) proteins were purchased form Proteintech company and dissolved in 50% glycerol-PBS. Then 1 µg GPAT1 and 1 µg PKA-Cα were incubated in the kinase assay buffer (20 mM Tris-HCl pH 7.5, 5 mM KCl, 5 mM DTT, 250 µM ATP) at 30 °C for 1 h. The reaction was terminated by adding SDS loading buffer, and the samples were loaded on SDS-PAGE gel and analyzed by Western blotting with indicated antibodies.

GPAT activity assay

GPAT activities were measured using spectrophotometric analysis, in accordance with previous studies[62,63]. Palmitoyl-CoA and glycerol-3-phosphate were used as substrates and the generation of CoA was monitored. Briefly, GPAT activity in whole-cell lysates or isolated liver mitochondria were assayed in a reaction mixture containing glycine (100 mM, pH 8.5), 0.5 mM EDTA, 1 mM DTT, 1 mM glycerol-3-phosphate (94124, Sigma-Aldrich), 0.1 mM palmitoyl-CoA (P9716, Sigma-Aldrich), and 0.1 mM 5, 5'-dithio-bis (2-nitrobenzoic acid) (DTNB). The reaction was started with the addition of 1 mM NADH and the formed DTNB-CoA complex was measured spectrophotometrically at 412 nm. In addition to the spectrophotometric assay, GPAT activity was also measured using UHPLC–MS/MS analysis. Briefly, GPAT activity in whole-cell lysates or isolated liver mitochondria was assayed in a reaction mixture containing 100 mM glycine (pH 8.5), 0.5 mM EDTA, 1 mM DTT, 1 mM glycerol-3-phosphate and 0.1 mM palmitoyl-CoA. The reaction was initiated by the addition of 1 mM NADH, and the resulting palmitoyl-LPA was quantified using UHPLC–MS/MS analysis.

PKA activity assay

Total cellular and mitochondrial PKA activities were measured by PKA Colorimetric Activity Kit (EIAPKA, Thermo Fisher) following manufacturers' instructions.

ACS activity assay

Acyl-CoA synthetase (ACS) was measured by a continuous coupled enzymatic assay as our previously described[14]. The reaction mixture included 100 mM Tris-HCl buffer (pH 8.0), 10 mM ATP, 15 mM MgCl$_2$, 5 mM dithiothreitol, 150 mM KCl, 1 mM potassium phosphoenolpyruvate (P7127, Sigma-Aldrich), 0.3 mM NADH in 100 mM triethanolamine (pH 8.2), and 500 µM sodium palmitate. 4.5 µg adenylate kinase (M3003, Sigma-Aldrich), 3 µg pyruvate kinase (P1506, Sigma-Aldrich), 3 µg lactate dehydrogenase (L8080, Solarbio), and 3 µg mitochondrial protein sample were added to a total reaction volume of 100 µL. After incubation at 37 °C for 1 min, the reaction was started by adding CoA (final concentration 600 µM) (C4282, Sigma-Aldrich). The absorbance changes at 334 nm were measured every 10 s for 15 min with a recording spectrophotometer. The reaction rate was determined using the slope and intercept from a NADH standard curve.

Measurement of mitochondrial membrane fluidity

Mitochondrial membrane fluidity was analyzed by fluorescence anisotropy of TMA-DPH probe (BB-48119, BestBio) according to the manufacturer's instructions. Isolated mitochondria (0.5 mg/mL) were labeled with TMA-DPH at a final concentration of 5 µM and incubated at 37 °C for 30 min. Fluorescence polarization value was measured using a fluorescence spectrometer (Jovin Yvon Horiba, Edison, NJ, USA), at an excitation wavelength of 355 nm and emission wavelength of 430 nm. Fluorescence anisotropy values calculated using the following equation: $P = (I_{VV} - G \times I_{VH})/(I_{VV} + G \times I_{VH})$; Direction calibration factor $G = I_{HV}/I_{HH}$. I_{VV}, I_{VH}, I_{HV} and I_{HH} represented the excitation and emission fluorescence intensity polarization in vertical (v) and horizontal (h), respectively. P value and membrane fluidity are negative correlation.

Hepatic VLDL-TG secretion analysis

Mice were fasted for 6 h and injected intraperitoneally with the lipase inhibitor Poloxamer-407 (P-407; 1 g/kg; Sigma-Aldrich). Blood was collected at baseline and at 1, 2 and 4 h after P-407 injection and plasma TG were quantified using a commercially available kit (290-63701 for TG, Wako; Tokyo, Japan).

Serum ketone bodies assay

Following the manufacturer's instructions, ketone bodies (acetoacetic acid and β-hydroxybutyric) were assessed using a readily accessible assay kit (EKBD-100, BioAssay Systems, USA).

Untargeted lipidomic analysis

Frozen liver (100 mg) was extracted by chloroform methanol (vol/vol, 2:1) method and dry in vacuum. Samples were dissolved in isopropanol for LC-MS (Suzhou Bionovogene). Chromatographic separation was accomplished in a Thermo Vanquish system equipped with an ACQUITY UPLC BEH C18 (100 × 2.1 mm, 1.7 µm, Waters) column. The ESI-MSn experiments were executed on the Thermo Q Exactive Focus mass spectrometer with the spray voltage of 3.5 kV and 2.5 kV in positive and negative modes, respectively. Analyzed and identified using LipidSearch software.

LC-MS/MS analysis of palmitoyl-carnitine

Quantitative analysis of palmitoyl-carnitine was performed using LC-MS/MS following our previously established methodology[14]. Liver tissues storaged at −80 °C after flash frozen in liquid nitrogen were submitted to Metware Biotechnology Co., Ltd. (Wuhan, China) for comprehensive analysis. The analytical platform consisted of a liquid chromatography electrospray ionization tandem mass spectrometry (LC-ESI-MS/MS) system, incorporating ultra-performance liquid chromatography (UPLC, Shim-pack), ultrafast liquid chromatography (UFLC, SHIMADZU CBM30A), and a triple quadrupole mass spectrometer (Applied Biosystems 6500 QTRAP). The quantification of palmitoyl-carnitine was achieved through scheduled multiple reaction monitoring (MRM) mode, ensuring high sensitivity and specificity in the detection process. Palmitoyl-carnitine standard was purchased from Sigma-Aldrich.

Ultra-high performance liquid chromatography/tandem mass spectrometry (UHPLC-MS/MS) for targeted analysis of LPA 16:0 and LPA 18:1

UHPLC–MS/MS analysis was performed by Beijing Scale Co., Ltd. (Beijing, China). LPA 16:0 (Cat. No. 857123) and LPA 18:1 (Cat. No. 857130) were purchased from Avanti Polar Lipids and used as the internal standard compound. Lipids were extracted from liver tissues, cells, isolated mitochondria and cell culture supernatant using 500 µL methanol/chloroform (1:1, vol/vol). The supernatant was precipitated in 300 µL of methanol-acetonitrile mixture. 50 ng/mL propranolol for positive ion mode. The extracts were filtered and separated (5 µL injection volume) on Acquity BEH C18 column (50 × 2.1 mm, 1.7 µm) at a flow rate of 0.25 mL/min at 40 °C. Analysis of LPA was performed using a Dionex UltiMate HPLC 3000 system equipped with a Thermo Q-Exactive mass spectrometer (Thermo Fisher Scientific, Bremen, Germany). The mobile phase was composed of 60% phase A (5 mM ammonium formiate and 0.1% formic acid in 50% water / 50% methanol) and 40% Phase B (100% acetonitrile), with a flow rate of 0.25 mL/min. The retention times of the analytes were between 4 to 5 min. After ionization by electrospray (ESI) in the mass spectrometer, the analytes were then separated according to known mass/charge ratios. Instrument control, data acquisition and analysis were performed using the Analyst 1.6.1 software. The LPA concentrations were calculated using standard curves derived from a mixture of purified LPA 16:0 and LPA 18:1. The following MS transitions for LPA 16:0: 411.25063/155.01044; LPA 18:1: 437.26627/155.01033; propranolol: 260.16451/116.10709 were recorded.

Public dataset collection

Public microarray dataset was collected from the NCBI GEO under accession number GSE135251 for analysis of mRNA expression levels of *Akap1*. Dataset inclusion criteria were 1) gene expression profiling was available; 2) the samples were largest.

Statistical analysis

Statistical analysis was performed using GraphPad Prism 8.0 (GraphPad Software Inc., La Jolla, CA). Results were expressed as mean ± SEM. Differences between two groups were analyzed using Student's t test. For comparisons among multiple groups, one-way and two-way ANOVA followed by Bonferroni post-tests were applied. All data were performed for statistical analysis. The correlation analysis was calculated with Pearson correlation coefficients.

Reporting summary

Further information on research design is available in the Nature Portfolio Reporting Summary linked to this article.

Data availability

The data that support the findings of this study are available within the article and supplementary information. Lipidomics data have been deposited in the Metabolights under the accession number MTBLS12350. Proteomics data have been deposited in the ProteomeXchange under the accession number PXD062388. Source data are provided with this paper.

References

1. Younossi, Z. et al. Global Perspectives on Nonalcoholic Fatty Liver Disease and Nonalcoholic Steatohepatitis. *Hepatology* **69**, 2672–2682 (2019).
2. Harrison, S. A. et al. A Phase 3, Randomized, Controlled Trial of Resmetirom in NASH with Liver Fibrosis. *N. Engl. J. Med.* **390**, 497–509 (2024).
3. Harrison, S. A. & Taub, R. A Phase 3 Trial of Resmetirom in NASH with Liver Fibrosis. Reply. *N. Engl. J. Med.* **390**, 1632–1633 (2024).
4. Friedman, S. L., Neuschwander-Tetri, B. A., Rinella, M. & Sanyal, A. J. Mechanisms of NAFLD development and therapeutic strategies. *Nat. Med.* **24**, 908–922 (2018).
5. Hammond, L. E. et al. Mitochondrial glycerol-3-phosphate acyltransferase-1 is essential in liver for the metabolism of excess acyl-CoAs. *J. Biol. Chem.* **280**, 25629–25636 (2005).
6. Neschen, S. et al. Prevention of hepatic steatosis and hepatic insulin resistance in mitochondrial acyl-CoA:glycerol-sn-3-phosphate acyltransferase 1 knockout mice. *Cell Metab.* **2**, 55–65 (2005).
7. Sveinbjornsson, G. et al. Multiomics study of nonalcoholic fatty liver disease. *Nat. Genet.* **54**, 1652–1663 (2022).
8. Ng, S. W. K. et al. Convergent somatic mutations in metabolism genes in chronic liver disease. *Nature* **598**, 473–478 (2021).
9. Jamialahmadi, O. et al. Exome-Wide Association Study on Alanine Aminotransferase Identifies Sequence Variants in the GPAM and APOE Associated With Fatty Liver Disease. *Gastroenterology* **160**, 1634–1646.e1637 (2021).
10. Liu, Y., Merrill, R. A. & Strack, S. A-Kinase Anchoring Protein 1: Emerging Roles in Regulating Mitochondrial Form and Function in Health and Disease. *Cells* **9**, https://doi.org/10.3390/cells9020298 (2020).
11. Bastola, T. et al. Role of A-Kinase Anchoring Protein 1 in Retinal Ganglion Cells: Neurodegeneration and Neuroprotection. *Cells* **12**, https://doi.org/10.3390/cells12111539 (2023).
12. Flippo, K. H. et al. AKAP1 Protects from Cerebral Ischemic Stroke by Inhibiting Drp1-Dependent Mitochondrial Fission. *J. Neurosci.* **38**, 8233–8242 (2018).
13. Narala, V. R. et al. Akap1 genetic deletion increases the severity of hyperoxia-induced acute lung injury in mice. *Am. J. Physiol. Lung Cell Mol. Physiol.* **314**, L860–L870 (2018).
14. Ji, L. et al. AKAP1 Deficiency Attenuates Diet-Induced Obesity and Insulin Resistance by Promoting Fatty Acid Oxidation and Thermogenesis in Brown Adipocytes. *Adv. Sci.* **8**, 2002794 (2021).
15. Schuster, S., Cabrera, D., Arrese, M. & Feldstein, A. E. Triggering and resolution of inflammation in NASH. *Nat. Rev. Gastroenterol. Hepatol.* **15**, 349–364 (2018).
16. Asgharpour, A. et al. A diet-induced animal model of non-alcoholic fatty liver disease and hepatocellular cancer. *J. Hepatol.* **65**, 579–588 (2016).
17. Dai, W. et al. Intracellular tPA-PAI-1 interaction determines VLDL assembly in hepatocytes. *Science* **381**, eadh5207 (2023).
18. Millar, J. S., Cromley, D. A., McCoy, M. G., Rader, D. J. & Billheimer, J. T. Determining hepatic triglyceride production in mice: comparison of poloxamer 407 with Triton WR-1339. *J. Lipid Res.* **46**, 2023–2028 (2005).
19. Pan, X. & Hussain, M. M. Bmal1 regulates production of larger lipoproteins by modulating cAMP-responsive element-binding protein H and apolipoprotein AIV. *Hepatology* **76**, 78–93 (2022).
20. Simon, J. et al. Magnesium accumulation upon cyclin M4 silencing activates microsomal triglyceride transfer protein improving NASH. *J. Hepatol.* **75**, 34–45 (2021).
21. Wendel, A. A., Cooper, D. E., Ilkayeva, O. R., Muoio, D. M. & Coleman, R. A. Glycerol-3-phosphate acyltransferase (GPAT)-1, but not GPAT4, incorporates newly synthesized fatty acids into triacylglycerol and diminishes fatty acid oxidation. *J. Biol. Chem.* **288**, 27299–27306 (2013).
22. Hoffman, N. J. et al. Global Phosphoproteomic Analysis of Human Skeletal Muscle Reveals a Network of Exercise-Regulated Kinases and AMPK Substrates. *Cell Metab.* **22**, 922–935 (2015).
23. Marchan, R. et al. Glycerol-3-phosphate Acyltransferase 1 Promotes Tumor Cell Migration and Poor Survival in Ovarian Carcinoma. *Cancer Res* **77**, 4589–4601 (2017).
24. Kersten, S., Desvergne, B. & Wahli, W. Roles of PPARs in health and disease. *Nature* **405**, 421–424 (2000).

25. Stapleton, C. M. et al. Lysophosphatidic acid activates peroxisome proliferator activated receptor-gamma in CHO cells that over-express glycerol 3-phosphate acyltransferase-1. *PLoS One* **6**, e18932 (2011).

26. Zimmermann, T. S. et al. Clinical Proof of Concept for a Novel Hepatocyte-Targeting GalNAc-siRNA Conjugate. *Mol. Ther.* **25**, 71–78 (2017).

27. Ahmad, M. & Hegele, R. A. Molecular Therapeutics in Development to Treat Hyperlipoproteinemia. *Mol. Diagn. Ther.*, https://doi.org/10.1007/s40291-024-00768-0 (2025).

28. Ellis, J. M. et al. Adipose acyl-CoA synthetase-1 directs fatty acids toward beta-oxidation and is required for cold thermogenesis. *Cell Metab.* **12**, 53–64 (2010).

29. Li, L. O. et al. Liver-specific loss of long chain acyl-CoA synthetase-1 decreases triacylglycerol synthesis and beta-oxidation and alters phospholipid fatty acid composition. *J. Biol. Chem.* **284**, 27816–27826 (2009).

30. Coleman, R. A. & Mashek, D. G. Mammalian triacylglycerol metabolism: synthesis, lipolysis, and signaling. *Chem. Rev.* **111**, 6359–6386 (2011).

31. Hammond, L. E. et al. Mitochondrial glycerol-3-phosphate acyltransferase-deficient mice have reduced weight and liver triacylglycerol content and altered glycerolipid fatty acid composition. *Mol. Cell Biol.* **22**, 8204–8214 (2002).

32. Wendel, A. A. et al. Glycerol-3-phosphate acyltransferase 1 deficiency in ob/ob mice diminishes hepatic steatosis but does not protect against insulin resistance or obesity. *Diabetes* **59**, 1321–1329 (2010).

33. Smith, K. R. et al. GPAT1 Deficiency in Mice Modulates NASH Progression in a Model-Dependent Manner. *Cell Mol. Gastroenterol. Hepatol.* **17**, 279–291 (2024).

34. Ellis, J. M. et al. Mice deficient in glycerol-3-phosphate acyltransferase-1 have a reduced susceptibility to liver cancer. *Toxicol. Pathol.* **40**, 513–521 (2012).

35. Tong, J. et al. Hepatic Interferon Regulatory Factor 6 Alleviates Liver Steatosis and Metabolic Disorder by Transcriptionally Suppressing Peroxisome Proliferator-Activated Receptor gamma in Mice. *Hepatology* **69**, 2471–2488 (2019).

36. Ning, Z. et al. USP22 regulates lipidome accumulation by stabilizing PPARgamma in hepatocellular carcinoma. *Nat. Commun.* **13**, 2187 (2022).

37. Zhang, Y. et al. Swimming exercise ameliorates insulin resistance and nonalcoholic fatty liver by negatively regulating PPARgamma transcriptional network in mice fed high fat diet. *Mol. Med.* **29**, 150 (2023).

38. Moolenaar, W. H. Development of our current understanding of bioactive lysophospholipids. *Ann. N.Y. Acad. Sci.* **905**, 1–10 (2000).

39. Sun, W. & Yang, J. Molecular basis of lysophosphatidic acid-induced NF-kappaB activation. *Cell Signal* **22**, 1799–1803 (2010).

40. Fan, G. et al. GPAT3 regulates the synthesis of lipid intermediate LPA and exacerbates Kupffer cell inflammation mediated by the ERK signaling pathway. *Cell Death Dis.* **14**, 208 (2023).

41. Sakuma, I. et al. Lysophosphatidic acid triggers inflammation in the liver and white adipose tissue in rat models of 1-acyl-sn-glycerol-3-phosphate acyltransferase 2 deficiency and overnutrition. *Proc. Natl Acad. Sci. USA* **120**, e2312666120 (2023).

42. Li, Z. et al. The ratio of phosphatidylcholine to phosphatidylethanolamine influences membrane integrity and steatohepatitis. *Cell Metab.* **3**, 321–331 (2006).

43. Vance, D. E. Phospholipid methylation in mammals: from biochemistry to physiological function. *Biochim. Biophys. Acta* **1838**, 1477–1487 (2014).

44. Klionsky, D. J. et al. Guidelines for the use and interpretation of assays for monitoring autophagy. *Autophagy* **8**, 445–544 (2012).

45. Bronnikov, G. E., Aboulaich, N., Vener, A. V. & Stralfors, P. Acute effects of insulin on the activity of mitochondrial GPAT1 in primary adipocytes. *Biochem. Biophys. Res. Commun.* **367**, 201–207 (2008).

46. Onorato, T. M., Chakraborty, S. & Haldar, D. Phosphorylation of rat liver mitochondrial glycerol-3-phosphate acyltransferase by casein kinase 2. *J. Biol. Chem.* **280**, 19527–19534 (2005).

47. Muoio, D. M., Seefeld, K., Witters, L. A. & Coleman, R. A. AMP-activated kinase reciprocally regulates triacylglycerol synthesis and fatty acid oxidation in liver and muscle: evidence that sn-glycerol-3-phosphate acyltransferase is a novel target. *Biochem. J.* **338**, 783–791 (1999).

48. Henriksen, B. S. et al. The effects of chronic AMPK activation on hepatic triglyceride accumulation and glycerol 3-phosphate acyltransferase activity with high fat feeding. *Diabetol. Metab. Syndr.* **5**, 29 (2013).

49. Cummings, D. E. et al. Genetically lean mice result from targeted disruption of the RII beta subunit of protein kinase A. *Nature* **382**, 622–626 (1996).

50. Feichtner, A. et al. Phosphorylation of the compartmentalized PKA substrate TAF15 regulates RNA-protein interactions. *Cell Mol. Life Sci.* **81**, 162 (2024).

51. Yang, J. D. et al. Gender and menopause impact severity of fibrosis among patients with nonalcoholic steatohepatitis. *Hepatology* **59**, 1406–1414 (2014).

52. Mills, E. L. et al. UCP1 governs liver extracellular succinate and inflammatory pathogenesis. *Nat. Metab.* **3**, 604–617 (2021).

53. Liu, D. et al. TNFAIP3 Interacting Protein 3 Overexpression Suppresses Nonalcoholic Steatohepatitis by Blocking TAK1 Activation. *Cell Metab.* **31**, 726–740.e8 (2020).

54. Kennedy, L. et al. Mast Cells Promote Nonalcoholic Fatty Liver Disease Phenotypes and Microvesicular Steatosis in Mice Fed a Western Diet. *Hepatology* **74**, 164–182 (2021).

55. Barbier-Torres, L. et al. Silencing hepatic MCJ attenuates non-alcoholic fatty liver disease (NAFLD) by increasing mitochondrial fatty acid oxidation. *Nat. Commun.* **11**, https://doi.org/10.1038/s41467-020-16991-2 (2020).

56. Wilfling, F. et al. Triacylglycerol synthesis enzymes mediate lipid droplet growth by relocalizing from the ER to lipid droplets. *Dev. Cell* **24**, 384–399 (2013).

57. Mendoza, R. et al. Isolation and Culture of Mouse Hepatocytes and Kupffer Cells (KCs). *Methods Mol. Biol.* **2455**, 73–84 (2022).

58. Colucci, S. et al. Liver Sinusoidal Endothelial Cells Suppress Bone Morphogenetic Protein 2 Production in Response to TGFbeta Pathway Activation. *Hepatology* **74**, 2186–2200 (2021).

59. Kleiner, D. E. et al. Design and validation of a histological scoring system for nonalcoholic fatty liver disease. *Hepatology* **41**, 1313–1321 (2005).

60. Sajiir, H. et al. Liver and pancreatic-targeted interleukin-22 as a therapeutic for metabolic dysfunction-associated steatohepatitis. *Nat. Commun.* **15**, 4528 (2024).

61. Shen, Y. et al. Ursodeoxycholic acid reduces antitumor immunosuppression by inducing CHIP-mediated TGF-beta degradation. *Nat. Commun.* **13**, 3419 (2022).

62. Krishnan, J. et al. Activation of a HIF1alpha-PPARgamma axis underlies the integration of glycolytic and lipid anabolic pathways in pathologic cardiac hypertrophy. *Cell Metab.* **9**, 512–524 (2009).

63. Wang, W. et al. Malonyl CoA Decarboxylase Inhibition Improves Cardiac Function Post-Myocardial Infarction. *JACC Basic Transl. Sci.* **4**, 385–400 (2019).

Acknowledgements

Author contributions

L.L.J. and J.L.X. designed the study; L.J.H., X.J.S., L.F.G., M.S.G., S.B.W. and Z.X.L. performed the animal experiments and liver histological analysis. L.J.H., X.J.S., R.L.L. and Y.Z.N. performed the cell experiments to investigate the mechanism; L.J.H., X.J.S., L.F.G. and H.T.G. recruited patients and collected clinical data; L.J.H., X.J.S., L.F.G. and M.S.G. analyzed data and drew the figures; L.L.J. and L.J.H. wrote the manuscript; L.L.J., J.L.X. and L.J.H. revised the manuscript; All authors have read and approved the article.

Competing interests

The authors declare no competing interests.

Additional information

Supplementary information The online version contains supplementary material available at
https://doi.org/10.1038/s41467-025-58790-7.

Correspondence and requests for materials should be addressed to Jinliang Xing or Lele Ji.

Peer review information *Nature Communications* thanks Eun Ju Bae, Magdalene Montgomery, and Kasparas Petkevicius for their contribution to the peer review of this work. A peer review file is available.

Reprints and permissions information is available at
http://www.nature.com/reprints

Publisher's note Springer Nature remains neutral with regard to jurisdictional claims in published maps and institutional affiliations.